Standard Title Page - Report on Federally Funded Project

1. Report No. FHWA/VTRC 06-R5	2. Government Accession No.	3. Recipient's Catalog No.
4. Title and Subtitle Creep and Fatigue Characteristics of Superpave Mixtures		5. Report Date September 2005
		6. Performing Organization Code
7. Author(s) Stacey Diefenderfer		8. Performing Organization Report No. VTRC 06-R5
9. Performing Organization and Address Virginia Transportation Research Council 530 Edgemont Road Charlottesville, VA 22903		10. Work Unit No. (TRAIS)
		11. Contract or Grant No. 75398
12. Sponsoring Agencies' Name and Address Virginia Department of Transportation FHWA 1401 E. Broad Street P.O. Box 10249 Richmond, VA 23219 Richmond, VA 23240		13. Type of Report and Period Covered Final
		14. Sponsoring Agency Code
15. Supplementary Notes		

16. Abstract

Laboratory creep and fatigue testing was performed on five Superpave surface hot-mix asphalt mixtures placed at the Virginia Smart Road. Differences in creep and fatigue response attributable to production and compaction methods were investigated. In addition, changes in creep response resulting from differences in specimen size were evaluated. Further, an evaluation of the effects of loading frequency, presence of rest periods, and specimen location within the pavement on fatigue life was conducted.

Creep compliance values were determined using viscoelastic-based calculations, and time-temperature superposition was used to generate mastercurves. Reported creep compliance response models from the literature were found inadequate for accurately describing the creep compliance mastercurves generated during this study. Differences in creep response between specimens of different sizes were found to be due to specimen and test variability, rather than size. An evaluation of the effects of laboratory and plant production and laboratory and field compaction was inconclusive as material variability appeared greater than production or compaction variability.

Simple regression models were found to be satisfactory for use in the development of prediction models for fatigue, although test data are necessary for calibration to particular mixture types. No relationships were found between fatigue model coefficients and volumetric properties of the mixtures tested because of the limited range of volumetric properties. Variability in volumetric properties between the mixtures produced at the plant and those produced to match the job mix formula did not significantly influence the predicted laboratory fatigue performance. Laboratory fatigue lives were similar between the laboratory-compacted fatigue specimens and specimens cut from the pavement; differences observed in performance were attributable to different air void contents. Predicted fatigue life was found to be statistically independent of the frequency of the applied loads or presence of rest periods for the mixtures, frequencies, and rest periods considered in this study. Minimal differences were observed between fatigue life predictions for plant-produced, field-compacted specimens cut from different locations in the pavement.

This study contributes to the understanding of the factors involved in creep and fatigue performance of asphalt mixtures. The mixture responses characterized by this study are related to the rutting and fatigue performance of asphalt pavements. The choice of appropriate asphalt materials to resist rutting and fatigue deterioration will result in reduced maintenance needs and longer service lives for pavements.

17 Key Words Superpave, creep, fatigue, indirect tensile creep, beam fatigue, hot mix asphalt	18. Distribution Statement No restrictions. This document is available to the public through NTIS, Springfield, VA 22161.		

19. Security Classif. (of this report)
  Unclassified
	20. Security Classif. (of this page)
	  Unclassified
		21. No. of Pages
		66
			22. Price

Form DOT F 1700.7 (8-72)   Reproduction of completed page authorized

FINAL REPORT

CREEP AND FATIGUE CHARACTERISTICS OF SUPERPAVE MIXTURES

Stacey Diefenderfer
Research Scientist

DISCLAIMER

The contents of this report reflect the views of the author, who is responsible for the facts and the accuracy of the data presented herein. The contents do not necessarily reflect the official views or policies of the Virginia Department of Transportation, the Commonwealth Transportation Board, or the Federal Highway Administration. This report does not constitute a standard, specification, or regulation.

ABSTRACT

Laboratory creep and fatigue testing was performed on five Superpave surface hot-mix asphalt mixtures placed at the Virginia Smart Road. Differences in creep and fatigue response attributable to production and compaction methods were investigated. In addition, changes in creep response resulting from differences in specimen size were evaluated. Further, an evaluation of the effects of loading frequency, presence of rest periods, and specimen location within the pavement on fatigue life was conducted.

Creep compliance values were determined using viscoelastic-based calculations, and time-temperature superposition was used to generate mastercurves. Reported creep compliance response models from the literature were found inadequate for accurately describing the creep compliance mastercurves generated during this study. Differences in creep response between specimens of different sizes were found to be due to specimen and test variability, rather than size. An evaluation of the effects of laboratory and plant production and laboratory and field compaction was inconclusive as material variability appeared greater than production or compaction variability.

Simple regression models were found to be satisfactory for use in the development of prediction models for fatigue, although test data are necessary for calibration to particular mixture types. No relationships were found between fatigue model coefficients and volumetric properties of the mixtures tested because of the limited range of volumetric properties. Variability in volumetric properties between the mixtures produced at the plant and those produced to match the job mix formula did not significantly influence the predicted laboratory fatigue performance. Laboratory fatigue lives were similar between the laboratory-compacted fatigue specimens and specimens cut from the pavement; differences observed in performance were attributable to different air void contents. Predicted fatigue life was found to be statistically independent of the frequency of the applied loads or presence of rest periods for the mixtures, frequencies, and rest periods considered in this study. Minimal differences were observed between fatigue life predictions for plant-produced, field-compacted specimens cut from different locations in the pavement.

This study contributes to the understanding of the factors involved in creep and fatigue performance of asphalt mixtures. The mixture responses characterized by this study are related to the rutting and fatigue performance of asphalt pavements. The choice of appropriate asphalt materials to resist rutting and fatigue deterioration will result in reduced maintenance needs and longer service lives for pavements. The elimination of only 10,000 tons of material found to be susceptible to premature deterioration could potentially save the Virginia Department of Transportation approximately $350,000 annually by reducing the resurfacing needs. As this is merely a fraction of the approximately 3.5 million tons of asphalt placed annually in Virginia, further gains in the understanding of rutting and fatigue processes and prevention of premature deterioration have great potential payoff over the long term.

FINAL REPORT

CREEP AND FATIGUE CHARACTERISTICS OF SUPERPAVE MIXTURES

Stacey Diefenderfer
Research Scientist

INTRODUCTION

Decreasing highway funding and increasing expectations for performance and quality have created a situation wherein it is particularly important for pavement engineers to understand the effects of asphalt mixture properties on pavement performance. Increasing traffic and decreasing maintenance funding are causing pavement deterioration to become more readily apparent. Part of the solution to deteriorating roadways is in the choice of better construction materials, which requires a greater understanding of the fundamental behavior and properties of such materials. Selection of appropriate highway materials with respect to climatic and loading conditions can greatly contribute to an increase in expected pavement service life and can lead to notable long-term national savings. With this in mind, the Virginia Department of Transportation (VDOT) adopted the use of Superpave asphalt mixtures in 1997.

Superpave mixtures are developed to perform under site-specific traffic and climatic loading conditions through a consideration of the interactions among climate, traffic, and pavement performance. They are designed to resist, in particular, deterioration in the form of low-temperature cracking, fatigue, and permanent deformation. Low-temperature cracking is caused by excessive tensile stresses induced over time by thermal gradients within pavements. Permanent deformation, commonly called rutting, is generally attributed to insufficiently designed pavements and is characterized as a permanent change in the form of a pavement or pavement layer. Fatigue is the process by which the pavement deteriorates through cracking because of small, built-up irrecoverable strains induced by repeated loading over time. In Virginia, low-temperature cracking has not been a significant issue, although rutting and fatigue have been identified as commonly occurring deterioration modes.

Two of the most problematic deterioration modes in asphalt pavements are permanent deformation and fatigue. The occurrence of these distresses may be reduced by the proper design of highway pavements, which requires comprehensive knowledge of the material properties and performance. As the properties of hot-mix asphalt (HMA) are significantly affected by specimen preparation, compaction, mixture inhomogeneity, and test method, a better understanding of the effects of these variables on response is needed.

The potential for rutting and fatigue is usually evaluated through laboratory testing of laboratory-produced specimens. However, production of laboratory specimens differs greatly from production of HMA for roadways. Differences have also been shown to exist between test results of specimens produced in the laboratory using different compaction methods and road cores (Button et al., 1994; Consuegra et al., 1989; Harvey and Monismith, 1993; Khan et al.,

1998; Masad et al., 1999). A comparison of compaction effects between the laboratory and field can yield valuable insight into adjusting design procedures such that in-situ material will more accurately reflect design performance.

Understanding the mechanisms of creep and fatigue is important for the design of effective pavement structures that resist deterioration. Testing was performed to evaluate the laboratory creep and fatigue response of Superpave surface mixtures that were placed at the Virginia Smart Road (Smart Road) in Blacksburg. The data collected include various mixture designs, volumetric properties, creep response, and fatigue response. Evaluation of the creep and fatigue performance of these mixtures enhances the understanding of the relationships between properties and performance for HMA mixtures. This understanding is expected to lead to more rational design methodologies for asphalt mixtures and pavement structures.

PURPOSE AND SCOPE

This report presents the findings of the evaluation of creep and fatigue performance of Superpave surface mixtures used at the Smart Road. The effects of differences in plant and laboratory production and in field and laboratory compaction were investigated. The effects of differences in mixture formulation and performance on creep and fatigue responses were also evaluated. Because of the small sample size, these experimental results are applicable only to the mixtures tested.

These findings are important as contributions to the understanding of appropriate mixture design and selection for improved pavement performance.

METHODS

Testing for the evaluation of creep and fatigue properties was performed on surface mixtures used at the Smart Road. Creep testing used the indirect tensile creep test on cylindrical specimens 100 mm and 150 mm in diameter. Fatigue testing used a third-point beam fatigue testing method under controlled strain conditions on rectangular beam specimens 50.8 mm by 63.5 mm by 381 mm.

Virginia Smart Road

Construction of the Smart Road began in 1997 to provide a direct connection between the town of Blacksburg and I-81. Through cooperation between Virginia Tech and VDOT, the Smart Road also became a test facility incorporating various types of transportation-related research. As part of this research, a pavement test facility was constructed. The facility is approximately 2.5 km in length, of which 1.3 km is flexible pavement divided into 12 test sections of approximately 100 m each. Each section is composed of a multi-layer pavement system and has a unique structural configuration.

The 12 configurations are designated as Sections A through L. Sections A through E are located in a fill area with a longitudinal slope of approximately 1% to 3.5%, and Sections F through L are located in a cut area with a longitudinal slope of approximately 4% to 6%. The configurations are shown in Table 1.

Six surface mixtures are employed among the 12 test sections, as indicated in Table 1:

1. Section A has SM-12.5D.
2. Sections B, E through H, and J have SM-9.5D.
3. Section C has SM-9.5E.
4. Section D and I have SM-9.5A.
5. Section K has an open-graded friction course (OGFC) surface.
6. Section L has SM-12.5.

The mixtures are designated by their use (surface mixture [SM]), nominal maximum aggregate size (12.5 mm and 9.5 mm), and performance-graded binder (PG 64-22, 70-22, and 76-22 as A, D, and E, respectively). The OGFC mixture found on the surface of Section K is designed to promote drainage and increase tire friction but was not evaluated during this study.

Table 1. Structural Configuration of Virginia Smart Road

Section	HMA Wearing Surface (mm)	HMA Intermediate Surface (mm)	HMA Base (BM-25.0) (mm)	HMA Surface (placed as base) (mm)	Asphalt-Stabilized OGDL (mm)	Cement-Stabilized OGDL (mm)	Cement-Stabilized Aggregate Base (mm)	21B Aggregate Base (mm)
A	38 SM-12.5D	-	150	-	75	-	150	175
B	38 SM-9.5D	-	150	-	75	-	150	175
C	38 SM-9.5E	-	150	-	75	-	150	175
D	38 SM-9.5A	-	150	-	75	-	150	175
E	38 SM-9.5D	-	225	-	-	-	150	75
F	38 SM-9.5D	-	150	-	-	-	150	150
G	38 SM-9.5D	-	100	50 SM-9.5A	-	-	150	150
H	38 SM-9.5D	-	100	50 SM-9.5A	75	-	150	75
I	38 SM-9.5A	-	100	50 SM-9.5A	75	-	150	75
J	38 SM-9.5D	-	225	-	75	-	-	150
K	19 OGFC	19 SM-9.5D	225	-	-	75	-	150
L	38 SMA-12.5	-	150	-	-	75	150	75

OGFC = open-graded friction course; OGDL = open-graded drainage layer.

Mixture Preparation

Specimens for testing were prepared from all surface mixtures except the OGFC found in Section K. Specimens had four designations, with the first term designating the production source and the second term designating the compaction location:

1. *Field-field specimens* were cores taken from the Smart Road and are representative of in-situ material.

2. *Field-lab specimens* were compacted in the laboratory from loose HMA gathered in the field at the time of construction of the Smart Road. These specimens were intended to be used to evaluate the differences between laboratory and field compaction.

3. *Lab-lab specimens* were laboratory prepared and compacted specimens that were prepared to match the mixture properties of the field-lab mixture. These properties were determined through ignition testing for asphalt content and sieve analysis for aggregate gradation. Lab-lab specimens were intended to be used to evaluate the effects of batch-plant and laboratory production practices on mixture response.

4. *Design-lab specimens* were laboratory prepared and compacted according to the original design batch sheets (job mix formulas) provided to the contractor by VDOT during construction of the Smart Road. These specimens were included to compare the performance of the designed mixture with that of the mixtures found in-place at the Smart Road.

Mixture designs and gradations for the specimens are presented in Appendix A.

Aggregate and binder were procured from the sources used during construction. Laboratory procedures for mixture preparation followed practices required by Superpave and VDOT. Mixtures were prepared in large batches to reduce variability attributable to batching and mixing. After mixing, HMA batches were placed in storage bags until compaction was performed; this was done so that compaction of the different sizes of gyratory specimens and beam specimens could be performed at different times. Bagged samples were stored at 25ºC. Aging as prescribed by Superpave was not performed before the HMA mixtures were bagged. Prior to compaction, bagged samples were aged in accordance with Superpave requirements, heated to compaction temperatures, and compacted into test specimens.

Indirect Tensile Specimens

Indirect tensile specimens used for creep compliance testing, with the exception of field-field specimens, were prepared in 100 mm and 150 mm diameter sizes (hereinafter referred to as 100 mm and 150 mm specimens). Field-field specimens were collected by coring the pavement at the Smart Road and then sawing off the surface layer. These specimens were obtained as 100 mm cores, as the surface layer at the Smart Road has an average thickness of 38 mm, which limits the dimensions of indirect tensile specimens. A summary of the creep test specimens is

presented in Table 2. Sets of 150 mm specimens were evaluated using two replicates, and sets of 100 mm specimens were composed of three replicates; this was done because the research team thought that the 100 mm specimens might have greater specimen-to-specimen variability because of the smaller sample mass. Field-field specimens were limited to two replicates because of restrictions placed on the quantity of cores taken from the Smart Road pavement.

The field-lab, lab-lab, and design-lab indirect tensile creep specimens were compacted using a Troxler Model 4140 gyratory compactor. Specimens were compacted to N_{design} as required by VDOT specifications. After compaction, volumetric analysis was performed on all specimens. Prior to testing, laboratory-produced specimens were saw-cut such that the height to diameter ratio was between 0.25 and 0.33, as required by AASHTO TP9-94. This was performed using a diamond-blade wet-saw, and the cuts were made to both specimen faces. This produced a smooth surface for test preparation. After cutting, specimens were dried to constant mass.

Specimens were prepared for testing by gluing small gage points to the specimen faces. Extensometer brackets were then mounted on the gage points and extensometers mounted to the brackets for testing. The gage points are approximately 3 mm thick and 7.5 mm in diameter. They were glued to the center of each specimen face using a cryanoacrylate adhesive such that the gage point spacing was 25.4 mm and 38.1 mm for the 100 mm and 150 mm specimens, respectively. After gluing, specimens were stored at 25ºC until testing commenced.

It is important to note that the adhesion of the gage points was greatly affected by the surface conditions of the sample being glued. Field-field samples were prepared with only one cut face because of the thin wearing surface layer at the Smart Road. These specimens were extremely difficult to glue, as the HMA macrotexture caused difficulty in obtaining a flat gluing surface and did not easily accept the adhesive; this meant that the uncut specimen face often had gage points that did not adhere well and were thus re-glued several times. This did not appear to affect subsequent deformation measurements adversely, except when the gage point detached during testing, but was a detriment to the timely performance of testing. The problem of the

Table 2. Summary of Indirect Tensile Creep Specimens

Mixture	Section	Field-Field 100 mm	Field-Lab		Lab-Lab		Design-Lab	
			100 mm	150 mm	100 mm	150 mm	100 mm	150 mm
SM-9.5A	D	2	3	2	3	2	3	2
	I[a]	2	3	2	3	2	3	2
SM-9.5D	B	2	3	2	3	2	3	2
	E	2	3	2	-	-	-	-
	F	2	3	2	-	-	-	-
	G	2	3	2	-	-	-	-
	H	2	3	2	-	-	-	-
	E-H	-	-	-	-	-	3	2
	J	2	3	2	-	-	3	2
SM-9.5E	C	2	3	2	3	2	3	2
SM-12.5D	A	2	3	2	3	2	3	2
SMA-12.5	L	2	3	2	3	2	3	2

[a]Designed with high laboratory compaction.

gage point detaching during testing rendered the results unusable; this was a disadvantage in the analysis of the field-field specimens as there was a limited number of measurements for consideration. From this experience, it was determined that saw-cutting of specimen faces is a necessity for the use of the extensometer mounting system employed in this study.

Beam Specimens

Beam specimens for fatigue testing were prepared as rectangular beams approximately 50.8 mm by 63.5 mm by 381 mm. The exceptions to this were the field-field beam specimens, which were approximately 35 to 45 mm in thickness, because of the thickness of the wearing surface at the Smart Road. A summary of fatigue testing specimens is presented in Table 3.

The field-lab, lab-lab, and design-lab beam fatigue specimens were compacted using an asphalt vibratory compactor by Pavement Technologies, Inc. After compaction, specimens were measured and weighed to determine their actual volumetric properties. Specimens were stored at 25ºC in a manner providing full support to prevent warping of the beams until testing.

Table 3. Summary of Fatigue Specimens

Mixture	Section	Field-Field	Field-Lab	Design-Lab	Lab-Lab
SM-9.5A	D	-	10	10	10
	I[a]	-	10	10	10
SM-9.5D	B	-	10	10	10
	E	-	10	-	-
	F	-	10	-	-
	G	-	10	-	-
	H	-	10	-	-
	E-H	-	-	-	10
	J	-	10	-	10
SM-9.5E	C	36	10	48	10
SM-12.5D	A	-	10	10	10
SM-12.5A	L	-	10	10	10

[a]Designed with high laboratory compaction.

Volumetric Analysis

The volumetric properties were determined for all gyratory specimens:

- asphalt content
- specific gravity of material components
- bulk density
- density at N_{ini}
- percent passing No. 200 sieve
- voids in total mix (VTM)
- voids in mineral aggregate (VMA)
- voids filled with asphalt (VFA)
- percent of maximum density at N_{ini}
- fines to asphalt (F/A) ratio.

Summaries of the volumetric properties for each mixture and the VDOT volumetric specification criteria are presented in Appendix B.

Test Procedures

Indirect Tensile Creep Test

Static creep behavior was characterized by performing the indirect tensile creep test. The indirect tensile creep test was chosen for two primary reasons. First, as the test setup is currently recommended for use in characterizing resilient modulus, it is readily available for use in creep analysis. The specimens required for this methodology are routinely produced in the laboratory, and field cores may also easily be tested as they conform to the geometry requirements. Second, the indirect tensile creep test is capable of evaluating the viscoelastic response of HMA. Using a 1000 sec loading time, the creep response may be measured at different temperatures and mastercurves created that allow for prediction of the response at very short or extended loading times. This allows for the determination of viscoelastic response over extended times without the difficulties of such extended laboratory testing. In this study, testing was performed using a loading time of 1000 sec and temperatures of 5ºC, 25ºC, and 40ºC; static loads were used and differed depending on the test temperature and specimen diameter. Specimen preparation and testing protocols were adapted from AASHTO TP 9-94, Determining the Creep Compliance and Strength of Hot-Mix Asphalt (HMA) Using the Indirect Tensile Test Device. Temperatures were chosen to consider a wide range of HMA creep response; the upper two temperatures are also comparable to pavement in-service temperatures wherein creep may be of concern.

Preliminary testing was performed to identify the required loading at each temperature. Previous research (Roque et al., 1995) has indicated that linear viscoelastic behavior is present up to a maximum strain level of approximately 2000 μstrain at low temperatures; thus, to prevent permanent damage, the upper goal of 500 μstrain was used for testing at 5ºC and 25ºC to allow the testing of each specimen at all temperatures. This significantly reduced the number of individual specimens required for testing. Table 4 identifies the loads used for creep testing at each temperature for the 100 mm and 150 mm specimens. During testing, deformation measurements were made on each face of the specimen in the horizontal and vertical directions. For analysis, these measurements were normalized to account for differences in the specimen thickness and averaged for each mixture at each temperature.

Table 4. Loads Used for Indirect Tensile Creep Test

Specimen	Temperature (ºC)	Load
100 mm field-field	5	900 N
	25	100 N
	40	20 N
100 mm	5	1700 N
	25	150 N
	40	30 N
150 mm	5	3000 N
	25	300 N
	40	40 N

Two methods of calculating the creep compliance were evaluated. Buttlar and Roque (1994) developed a method of analysis for creep data at temperatures below 0ºC using finite element analysis of diametrically loaded cylindrical specimens. This method is endorsed in AASHTO TP9-94. The creep compliance is calculated as follows:

$$D(t) = \frac{H(t)_{TRIM} \cdot d_{avg} \cdot t_{avg}}{P_{avg} \cdot GL} \cdot C_{CMPL}$$

[Eq. 1]

where

$D(t)$ = creep compliance
$H(t)_{TRIM}$ = trimmed mean horizontal deflection, mm
d_{avg} = average specimen diameter, mm
t_{avg} = average specimen thickness, mm
P_{avg} = average creep load, kN
GL = gage length over which deflections are measured, mm
C_{CMPL} = compliance factor.

The compliance factor, C_{CMPL}, is related to the horizontal and vertical deflections through Eq. 2:

$$C_{cmpl} = 0.6354 \left(\frac{X}{Y} \right)^{-1} - 0.332$$

[Eq. 2]

where X/Y is the absolute value of the ratio of the measured horizontal deflection to the measured vertical deflection. The compliance factor is restricted by the following limits, based on restrictions placed on Poisson's ratio:

$$\left[0.704 - 0.213 \left(\frac{t_{avg}}{d_{avg}} \right) \right] \leq C_{CMPL} \leq \left[1.566 - 0.195 \left(\frac{t_{avg}}{d_{avg}} \right) \right]$$

[Eq. 3]

$$0.20 \leq \frac{t_{avg}}{d_{avg}} \leq 0.65$$

[Eq. 4]

Poisson's ratio is calculated as (Buttlar and Roque, 1994):

$$\nu = -0.10 + 1.480 \cdot \left(\frac{X}{Y} \right)^2 - 0.778 \cdot \left(\frac{t}{d} \right)^2 \left(\frac{X}{Y} \right)^2$$

[Eq. 5]

where ν is Poisson's ratio. Poisson's ratio is restricted such that $0.05 \leq \nu \leq 0.50$ to prohibit unrealistic values from entering into other calculations. The upper limit coincides with the upper

bound of Poisson's ratio for elastic materials. The lower limit was introduced to keep compliance values within reasonable limits for unrealistic X/Y values.

An alternative method of analysis was developed and presented that uses a viscoelastic determination of the creep compliance (Kim et al., 2002; Wen and Kim, 2002). This method was developed to evaluate the viscoelastic response used in fatigue characterization and was used to evaluate testing performed at temperatures between −10°C and 30°C. The elastic-viscoelastic correspondence principle was used to obtain viscoelastic solutions from the elastic equations. This principle states that the viscoelastic equations are equivalent to the elastic equations in the Laplace transformed domain. After several calculations, the creep compliance is expressed as:

$$\nu = -\frac{a_1 \; U(t) + b_1 \; V(t)}{a_2 \; U(t) + b_2 \; V(t)}$$

[Eq. 6]

$$D(t) = -\frac{d}{P}[c \; U(t) + e \; V(t)]$$

[Eq. 7]

where a_1, a_2, b_1, b_2, c, and e are coefficients related to the specimen diameter and gage length of the displacement measurements and are shown in Table 5.

To facilitate the process of time-temperature superposition, the compliance isotherms were presmoothed prior to shifting. This process is recommended for use with experimental data gathered on asphalt mixtures because it is subject to the variance associated with the intrinsic inhomogeneity of the mixture. Buttlar et al. (1998) suggested the use of a second-degree polynomial for presmoothing log-transformed creep compliance data. The function is expressed as:

$$\log D(t) = \beta_0 + \beta_1 \cdot \log(t) + \beta_2 \cdot (\log(t))^2$$

[Eq. 8]

where β_0, β_1, and β_2 are regression constants. This model was used satisfactorily to provide presmoothing prior to performing time-temperature superposition.

After evaluation of the presmoothed compliance values at each test temperature, compliance curves were shifted to a reference temperature, T_{ref}, to form a single mastercurve using the principle of time-temperature superposition. An example of time-temperature superposition is shown in Figure 1. The required amount of shift at each temperature is considered the shift factor, a_T, and is defined as a constant by which loading times at the

Table 5. Coefficients for Use in Equations 6 and 7

Specimen	Gage Length	a_1	a_2	b_1	b_2	c	e
100	25.4	3.385	3.136	1.000	3.124	0.7875	2.2795
150	38.1	3.363	1.082	1.000	3.100	0.7947	2.2769

particular temperature must be divided to give the reduced time, t_r, at which the corresponding point may be found on the mastercurve. The reduced time is described mathematically as:

$$t_r = \frac{t}{a_T}$$

[Eq. 9]

where

   t_r = reduced time, sec
   t = loading time at the particular temperature, sec
   a_T = shift factor.

Previous research on asphalt binders (Christensen and Anderson, 1992) has suggested that the relationship between log (a_T) and temperature, T, varies linearly at temperatures below about 0ºC. This relationship is also supported for asphalt mixtures at low to intermediate temperatures (Christensen, 1998):

$$\log(a_T) = C_1 + C_2T$$

[Eq. 10]

where

   T = temperature of the shifted data
   C_1 and C_2 = constants describing the slope and intercept of the relationship.

This relationship was found to be satisfactory for the description of shift factors in this research.
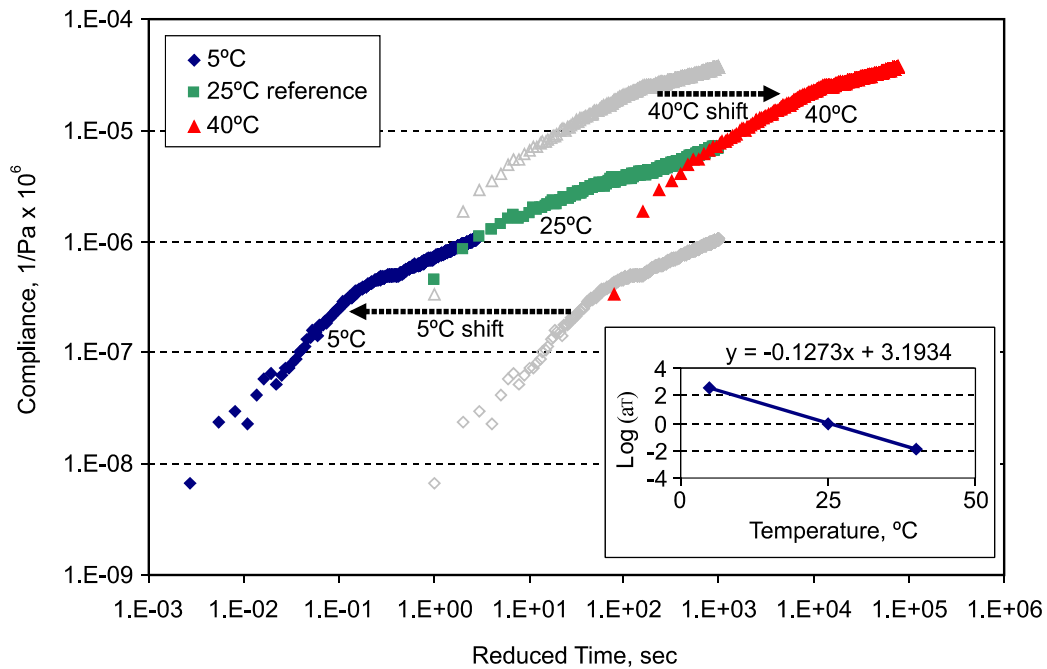
Figure 1. Example of Time-Temperature Superposition

10

Third-Point Beam Fatigue Test

Fatigue life testing was performed using the third-point mode of loading flexural test under controlled-strain conditions, as specified in the AASHTO TP8-94 protocol. This method of testing was chosen because of its ease of use and understanding and its adoption as a standard. In pavement analysis, generally, conditions of stress-control may be assumed to represent in-situ response as the surface course is considered to be integral with the base course, creating a thick-layer system. However, as this study sought to quantify properties of the surface mixtures individually, the researcher felt that following the recommended AASHTO test method was appropriate.

The third-point beam fatigue test applies loading at points located at one-third distances from the beam ends. This produces uniform bending in the central third of the specimen and significantly simplifies analysis. The test is run until failure occurs; however, there is dispute concerning the definition of failure for the controlled strain test, as it is very difficult to reach a physical failure via fracture. The AASHTO specification sets the criterion for failure as occurring when there is a 50% reduction in the measured stiffness; initial stiffness is measured after 50 applied load cycles. "True failure" in fatigue has been shown to be correlated strongly with the 50% reduction of initial stiffness (Carpenter et al., 2003):

$$N_{\text{true failure}} = 21758 + 1.30727 \cdot N_{50\% \text{ K}} \quad R^2 = 0.91 \qquad \text{[Eq. 11]}$$

where

$N_{\text{true failure}}$ = number of cycles to failure
$N_{50\% \text{ K}}$ = number of cycles required to reduce the initial stiffness by 50%.

This method of failure definition was chosen to comply with specifications and to provide a standard method of test comparable to that performed by other researchers in the assumption that future comparisons may be made. In addition, although fatigue life response will be different depending on the mode of loading, the overall rankings of mixtures are not significantly changed because of the mode of loading (Strategic Highway Research Program, 1994).

Fatigue testing was performed on the specimens listed in Table 3. Fatigue beams cut from the Smart Road (designated section C, mixture SM-9.5E, field-field) were evaluated by location and with respect to the direction of compaction; wheelpath and center-of-lane specimens reflect the effect of traffic compaction, whereas beams cut with the longitudinal length parallel with or perpendicular to traffic reflect the effect of construction compaction, as the roller compacts mixtures parallel with the roadway direction. In addition, evaluations of loading frequency and rest period effects were performed by evaluating specimens using three load frequencies and two rest period lengths, summarized in Table 6. These combinations were evaluated for only one surface mixture, SM-9.5E, located in section C, and one production condition, design-lab.

Table 6. Summary of Loading Frequencies and Rest Periods to Be Tested

Load Frequency	Rest Period
10 Hz	-
5 Hz	-
1 Hz	-
10 Hz	0.4 sec
10 Hz	0.9 sec

Tests were performed at 25ºC. The strain levels for the replicate sets of four specimens each were chosen such that the specimen life ranged from approximately 5,000 to 300,000 cycles, with the failure criterion being 50% reduction of the initial stiffness. Testing was performed in the controlled-strain mode of loading at a frequency of 10 Hz, with the exception of the testing designed to evaluate frequency and rest period changes. Results from each set of tests were used in calculating resulting stresses, strains, stiffness, and dissipated energy at each load cycle.

The peak-to-peak stress is computed as:

$$\sigma_t = \frac{3 a P}{w h^2}$$

[Eq. 12]

where

σ_t = peak-to-peak maximum tensile stress, N
a = L/3, mm
L = beam span, mm
P = applied peak-to-peak load, N
w = beam width, mm
h = beam height, mm.

Peak-to-peak strain is determined as:

$$\varepsilon_t = \frac{12 h \delta}{3 L^2 - 4 a^2}$$

[Eq. 13]

where
ε_t = peak-to-peak maximum tensile strain, mm/mm
δ = beam deflection at neutral axis, mm.

Stiffness is calculated as follows:

$$S = \frac{\sigma_t}{\varepsilon_t}$$

[Eq. 14]

where S is the beam stiffness in Pa.

The phase angle is expressed as:

$$\phi = 360 \cdot f \cdot s$$

[Eq. 15]

where

ϕ = phase angle, º
f = load frequency, Hz
s = time lag between P_{max} and δ_{max}, sec.

Dissipated energy per cycle is computed as:

$$D = \pi \sigma_t \varepsilon_t \sin \phi$$

[Eq. 16]

where D is the dissipated energy per cycle, expressed in Pa. The cumulative dissipated energy was determined by summing the dissipated energy per cycle over the life of the specimen.

RESULTS AND DISCUSSION

Creep Response Evaluation

The potential for increased tendency of permanent deformation was evaluated through the use of the indirect tensile creep test. Raw data collected from the testing included time, applied load, and vertical and horizontal deflections. These were used to calculate the creep compliance as a function of time for each specimen set.

Methods of Calculation

Two methods of calculation for the creep compliance were considered. The first assumes elastic behavior of the asphalt mixture and was recommended by Buttlar and Roque (1994) for use when testing mixtures at or below 0ºC; calculations were presented in Eqs. 1 through 5. The second, presented by Kim et al. (2002) and Wen and Kim (2002), uses a viscoelastic determination of the creep compliance, as shown in Eqs. 6 and 7, and was shown suitable for use at temperatures between –10 ºC and 30ºC.

The decision was made to use Eqs. 6 and 7 for evaluation of the creep compliance and Poisson's ratio; the equations were chosen for several reasons. First, evaluation of the ratio of horizontal to vertical deformations (X/Y ratio, used in Eqs. 2 and 5) for specimens tested during this study indicated that the X/Y values exceed the ranges acceptable for use with the Buttlar and Roque (1994) methodology. These ranges were recommended to prevent Poisson's ratio from exceeding the range of 0.05 to 0.50. Further, the test temperatures in this study were closer to the range used by Kim et al. (2002) and Wen and Kim (2002). Finally, it was believed that the test temperatures were likely to result in non-elastic response of the HMA, and as such the viscoelastic equations were thought to describe the mixture response better.

13

During analysis of the data, values of Poisson's ratio calculated with Eq. 7 were found to be outside the range of acceptable values for almost every specimen set at every temperature. Poisson's ratios with negative values and with values as high as 500 were calculated. As neither of these scenarios is phenomenologically acceptable, the measurements taken from the indirect tensile creep test in this study may not be appropriate for the determination of Poisson's ratio. Thus, further evaluation of the Poisson's ratio from this study was discontinued.

Mastercurve Generation

Mastercurves were generated from pre-smoothed compliance data using time-temperature superposition. The rheology analysis program IRIS was used to perform time-temperature superposition. The shift factors generated were used to verify the relationship presented in Eq. 10. Mastercurve and shift factor data are available from the author by request.

It was intended that a deliverable of this project would be a validated model form for creep compliance that would allow for quantifiable comparison of mixtures. Several models presented in the literature were considered; however, none resulted in successful modeling of the creep compliance mastercurves resulting from this study. Because of time constraints, modeling efforts were finally terminated and directed toward qualitative analysis.

<div align="center">

Creep Performance of Mixtures

</div>

As modeling was unsuccessful, qualitative evaluation of the creep response to identify the potential increased tendency of mixtures to experience permanent deformation was performed. Compliance values for mixtures were compared to investigate the influence of specimen size and production and compaction methods.

Effects of Specimen Size

Initial evaluation of the creep response was performed to investigate potential differences in creep response attributable to specimen size; 100 mm and 150 mm specimens were prepared. Thickness to diameter ratios were maintained in the range of 0.25 to 0.33 for each specimen set. Volumetric properties, including air voids, were similar for the specimen sets. Calculations of compliance values were universal, as equations included factors to account for specimen diameter and thickness.

There were differences in creep response between the 100 mm and 150 mm specimens; however, the significance of the differences was not determined. A typical comparison between responses is shown in Figure 2. Differences were quantified by determining the average difference as a percentage of the compliance values for the 150 mm specimens for each temperature. The values for the 150 mm specimens were used as a reference, since this is the diameter specified in AASHTO TP 9-94. Figure 3 illustrates the change in percent difference at various times throughout the test duration. As can be seen, although the average difference at each temperature gives an indication of the changes in response between the 100 mm and 150 mm specimens, it does not fully characterize those differences, as they vary considerably during
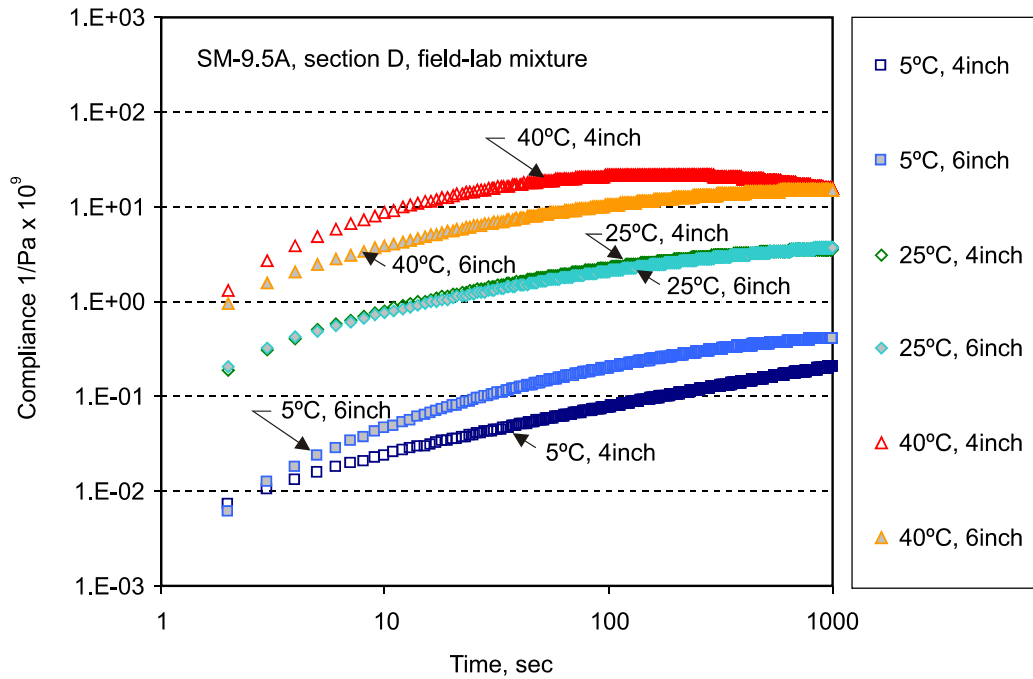
Figure 2. Creep Compliance Curves for SM-9.5A, Field-Lab, Section D: 100 mm and 150 mm Specimen Sets
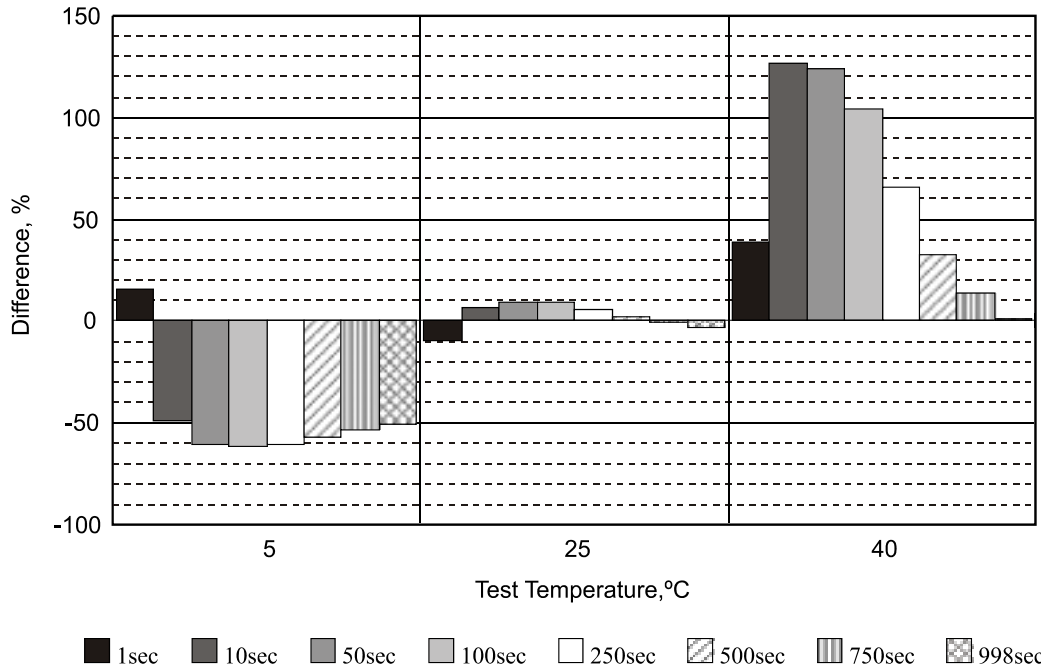
Figure 3. Percent Difference in Creep Compliance: SM-9.5A, Field-Lab, Section D, at Various Test Times: 100 mm and 150 mm Specimen Sets

the duration of the test. The response at 1 sec loading time is shown to vary considerably from the trend beginning with the 10 sec load data. This may be due to instability in the loading at 1 sec and delayed response of the specimen, as the servohydraulic equipment used cannot provide instantaneous loading and uses a very steep ramp loading to attempt to achieve instantaneous response.

15

Table 7 summarizes the average percent difference in compliance values between the sample sizes for each mixture at each temperature. It can be seen that average differences range from a minimum absolute difference of 2% to a maximum absolute difference of 18,366%. Positive values indicate that the compliance values for the 150 mm specimens were greater than for the 100 mm specimens; negative values indicate the reverse. There were no obvious trends seen in the average percent difference for mixture type, production method, or test temperature. The results of this analysis imply that the differences in response seen from the two specimen sets are most likely a result of specimen and test variability, since the calculation of creep compliance from deformations is weighted to account for specimen diameter and height.

Table 7. Summary of Average Percent Differences in Creep Compliance Between 100 mm and 150 mm Specimen Sets

Mixture	Section	Design-Lab			Field-Lab			Lab-Lab		
		5ºC	25ºC	40ºC	5ºC	25ºC	40ºC	5ºC	25ºC	40ºC
SM-9.5A	D	371	21	-58	-56	2	43	-58	-6	178
	I	-59	-71	-60	22	97	66	9	-50	-59
SM-9.5D	B				-49	-84	-9	161	-26	285
	E				-87	-73	-68			
	F	64	65	13	-64	-39	2	-23	63	43
	G				19	3	159%			
	H				-39	-55	-54			
	J				21	-28	-51	3	101	146
SM-9.5E	C	201	253	-11	-52	3	12	-20	15	-20
SM-12.5D	A	128	15	-8	4	1198	18366	50	151	167
SMA-12.5	L	74	89	-32	-36	-13	24	41	132	295

Effects of Production Method

To evaluate the effects on creep response attributable to production method, comparisons were made between plant-produced and laboratory-produced mixtures that were compacted into test specimens in the laboratory. Specimen sets with a diameter of 150 mm were used for this comparison, as this diameter is specified as standard size test specimens in AASHTO TP 9-94. The basis for the percentage difference computation was taken to be the field-lab specimen set, as these samples were prepared from the plant-produced material placed in the field.

The first comparison considered the field-lab and lab-lab specimen sets. The lab-lab specimen set was produced with the intent to match the asphalt content and gradation of the loose plant-produced mixture. Unfortunately, the asphalt content match was not exact for some mixtures; therefore, there may be some influence attributable to the difference; however, the maximum difference was 0.6%, with 7 of the 11 sections having differences less than or equal to 0.3%, as shown in Table 8. This comparison was intended to evaluate the effects of production methods on the response on specimen sets having equivalent volumetric properties.

Average percent differences in the creep compliance for each section and temperature are presented in Table 9. The results indicate greater differences on average for the SM-9.5A and

Table 8. Asphalt and Air Void Contents: Field-Lab and Lab-Lab Specimen Sets

Mixture	Section	% Asphalt		VTM (%)	
		Field-Lab	Lab-Lab	FL	LL
SM-9.5A	D	6.3	6.8	1.3	0.9
	I	5.4	5.3	1.5	6.0
SM-9.5D	B	4.7	5.4	3.6	1.8
	E	5.9	6.0	1.4	1.9
	F	5.4		3.6	
	G	6.3		3.6	
	H	5.6		4.1	
	J	4.9	5.1	7.5	4.6
SM-9.5E	C	5.8	6.0	2.3	2.0
SM-12.5D	A	5.9	5.9	3.2	5.2
SMA-12.5	L	6.8	6.4	1.8	1.8

Table 9. Summary of Average Percent Differences in Creep Compliance Between Field-Lab and Lab-Lab Specimen Sets

Mixture	Section	5ºC	25ºC	40ºC
SM-9.5A	D	221	136	186
	I	-153	-305	-556
SM-9.5D	B	79	86	84
	E	59	82	79
	F	26	23	48
	G	89	23	17
	H	7	65	79
	J	-49	46	81
SM-9.5E	C	25	26	26
SM-12.5D	A	74	-98	-2646
SMA-12.5	L	-86	-47	26

SM-12.5D mixtures. The differences in asphalt or air void content, shown in Table 8, do not appear to explain this difference, as there were similar discrepancies in the asphalt and air void contents with other mixtures. Detailed results of the comparison analysis of compliance differences are shown in Table 10. These results indicate that there are not unique trends in the response for the different mixtures, except that values in the mid-range of time, between approximately 50 and 750 sec, appear to be fairly constant for most mixtures.

The second comparison considered the field-lab and design-lab specimen sets. The field-lab specimen sets were again considered the basis for the comparison. The design-lab specimens were produced using the gradation and asphalt content from the job mix batch sheets, with no consideration given to the properties of the plant-produced mixtures. The purpose of the comparison was to evaluate the differences expected between plant and laboratory production of the design mixtures.

The comparison of the volumetric properties of the two specimen sets is shown in Table 11, where it can be seen that asphalt contents were the same for two mixtures but different for the remaining mixtures (0.3% to 0.6%). Air voids were variable between the two production sets; with the exception of the SM-9.5E mixture, design-lab specimens had higher air void

Table 10. Summary of Percent Differences in Creep Compliance Between Field-Lab and Lab-Lab Specimen Sets at Various Times

Mixture	Section	Temp.	1 sec	10 sec	50 sec	100 sec	250 sec	500 sec	750 sec	998 sec
SM-9.5A	D	5ºC	-79	-91	-124	-147	-188	-231	-261	492
		25ºC	-251	-167	-141	-135	-132	-134	-136	13
		40ºC	-83	-143	-174	-182	-189	-189	-188	62
	I	5ºC	81	-21	-138	-173	-184	-163	-140	73
		25ºC	-128	-145	-187	-215	-266	-318	-355	75
		40ºC	-38	-189	-338	-411	-512	-590	-635	75
SM-9.5D	B	5ºC	59	82	85	85	82	79	76	55
		25ºC	45	76	84	85	86	86	86	23
		40ºC	93	89	87	86	85	84	84	64
	E	5ºC	49	75	76	74	68	58	50	86
		25ºC	56	77	82	82	83	82	81	78
		40ºC	55	82	85	85	82	79	75	70
	F	5ºC	74	61	48	41	32	23	18	59
		25ºC	-11	27	34	33	28	22	17	53
		40ºC	54	75	74	70	61	47	35	31
	G	5ºC	127	98	89	87	87	88	90	5
		25ºC	8	29	34	33	29	22	17	19
		40ºC	51	53	46	39	26	12	1	129
	H	5ºC	81	36	15	8	0	5	8	50
		25ºC	31	65	70	70	68	65	62	58
		40ºC	88	91	90	88	84	78	73	47
	J	5ºC	-661	-296	-151	-106	-58	-30	-16	1
		25ºC	39	36	38	40	43	46	49	33
		40ºC	37	72	79	81	82	81	81	47
SM-9.5E	C	5ºC	28	29	28	27	26	25	24	247
		25ºC	11	21	25	26	27	27	26	241
		40ºC	41	27	22	22	23	26	28	22
SM-12.5D	A	5ºC	36	75	80	80	78	75	71	49
		25ºC	-345	-220	-156	-134	-107	-89	-80	696
		40 ºC	-4871	-3711	-3142	-2942	-2712	-2561	-2481	-2428
SMA-12.5	L	5 ºC	55	18	-20	-40	-70	-96	-112	123
		25 ºC	-28	-29	-34	-38	-43	-48	-52	54
		40ºC	-501	-31	25	33	34	29	24	18

Table 11. Asphalt and Air Void Contents for Field-Lab and Design-Lab Specimen Sets

Mixture	Section	% Asphalt		VTM (%)	
		Field-Lab	Design-Lab	Field-Lab	Design-Lab
SM-9.5A	D	6.3	6.3	1.3	3.6
	I	5.4	5.4	1.5	4.3
SM-9.5D	B	4.7	5.3	3.6	5.0
SM-9.5E	C	5.8	6.2	2.3	1.3
SM-12.5D	A	5.9	5.6	3.2	4.8
SMA-12.5	L	6.8	6.3	1.8	2.3

contents than their field-lab counterparts. This does not appear to have had a definitive effect on the compliance results, as can be seen in Table 12, where positive differences indicate higher compliance response values for field-lab specimen sets and negative percentages indicate lower values for field-lab specimens than for design-lab specimens. Table 12 also indicates a lack of general trends in the averaged response values. The percent difference in response at varying test times is summarized in Table 13, where no trends are evident.

Table 12. Summary of Average Percent Differences in Creep Compliance Between Field-Lab and Design-Lab Specimen Sets

Mixture	Section	5ºC	25ºC	40ºC
SM-9.5A	D	27	-104	-607
	I	-468	-117	-78
SM-9.5D	B	-21	66	42
SM-9.5E	C	24	60	-24
SM-12.5D	A	-3	-1063	-7311
SMA-12.5	L	-32	-90	-106

Table 13. Summary of Percent Differences in Creep Compliance Between Field-Lab and Design-Lab Specimen Sets at Various Times

Mixture	Section	Temp.	1 sec	10 sec	50 sec	100 sec	250 sec	500 sec	750 sec	998 sec
SM-9.5A	D	5ºC	-437	-49	13	24	31	31	29	492
		25ºC	-176	-119	-103	-100	-100	-103	-106	13
		40ºC	-778	-585	-549	-553	-577	-610	-637	62
	I	5ºC	35	-327	-646	-682	-596	-457	-363	-297
		25ºC	-55	-88	-105	-111	-117	-120	-121	-121
		40ºC	-35	-49	-60	-66	-74	-80	-84	-87
SM-9.5D	B	5ºC	-4	23	19	12	-4	-24	-40	55
		25ºC	59	69	70	70	68	66	64	23
		40ºC	-67	-67	-21	3	33	52	61	64
SM-9.5E	C	5ºC	20	15	16	18	21	25	27	247
		25ºC	42	56	60	61	61	60	60	241
		40ºC	-7	-19	-24	-25	-25	-25	-24	22
SM-12.5D	A	5ºC	-7	34	35	29	14	-5	-21	-35
		25ºC	-568	-622	-740	-819	-959	-1099	-1198	-1277
		40ºC	-6572	-8802	-8987	-8657	-7892	-7124	-6622	-6252
SMA-12.5	L	5ºC	81	47	12	-5	-26	-39	-46	-50
		25ºC	-132	-137	-123	-114	-99	-86	-78	-72
		40ºC	70	11	-48	-74	-102	-116	-122	-123

In summary, evaluation of the effects of laboratory and plant production was inconclusive. Differences in volumetric quantities (asphalt content and air void content) may be contributing to the inconsistent comparisons, but it is more likely that material variability is simply greater than production variability for the mixtures and materials used in this study.

Effects of Differences in Compaction Methods

The effects on creep response due to differences in roller compaction and gyratory compaction were considered by comparing the test results for field-field and field-lab specimens.

Specimen sets with diameters of 100 mm were used for this comparison, as the pavement cores were not sufficiently thick to evaluate as a 150 mm specimen. The basis for the percentage difference computation was taken to be the field-field specimen set, as these samples correspond to the in-situ HMA.

The comparison of volumetric properties is shown in Table 14, where it can be seen that all mixtures have equivalent asphalt contents, although differences in air voids are seen because of the different compaction methods. Except for the SM-9.5A mixture from section I, the laboratory specimens had lower air void contents than did the field cores. This is due in part to the fact that laboratory specimens were produced to simulate air void contents under traffic whereas the field specimens were sampled prior to the application of traffic. Comparisons of the differences in creep compliance are presented in Tables 15 and 16, which show the summary of average differences and time-dependent differences, respectively. Again, no trends are evident.

In summary, results from the creep evaluation did not lead to decisive conclusions concerning the effects of production and compaction methods or the influence of specimen size. It appeared that each variable investigated should have had a specific, quantifiable influence on creep response, but due to the apparent variability in the materials used, these influences were not seen.   In future evaluation, consideration should be given to the use of different test methods that may be more discriminating at the chosen test temperatures.

Table 14.   Asphalt and Air Void Contents for Field-Field and Field-Lab Specimen Sets

Mixture	Section	% Asphalt		VTM (%)	
		Field-Field	Field-Lab	Field-Field	Field-Lab
SM-9.5A	D	6.3	6.3	1.9	1.3
	I	5.4	5.4	1.1	1.5
SM-9.5D	B	4.7	4.7	8.6	3.6
	E	5.9	5.9	4.8	1.4
	J	4.9	4.9	10.6	7.5
SM-9.5E	C	5.8	5.8	6.0	2.3
SM-12.5D	A	5.9	5.9	5.8	3.2
SMA-12.5	L	6.8	6.8	7.3	1.8

Table 15. Summary of Average Percent Differences in Creep Compliance Between Field-Field and Field-Lab Specimen Sets

Mixture	Section	5ºC	25ºC	40ºC
SM-9.5A	D	95	94	92
	I	33	24	61
SM-9.5D	B	45	-17	-164
	E	89	63	69
	J	72	40	-74
SM-9.5E	C	81	78	65
SM-12.5D	A	39	59	-238
SMA-12.5	L	93	91	86

Table 16. Summary of Percent Differences in Creep Compliance Between Field-Field and Field-Lab Specimen Sets at Various Times

Mixture	Section	Temp.	1 sec	10 sec	50 sec	100 sec	250 sec	500 sec	750 sec	998 sec
SM-9.5A	D	5°C	65	88	93	94	95	95	95	95
		25°C	91	93	94	94	94	94	94	94
		40°C	89	90	91	91	92	92	93	93
	I	5°C	25	45	47	45	39	32	27	22
		25°C	-136	-38	-1	10	21	28	32	34
		40°C	85	80	74	71	65	60	56	53
SM-9.5D	B	5°C	78	59	47	45	43	44	46	47
		25°C	35	-79	-104	-86	-43	-6	15	28
		40°C	-1101	-487	-287	-231	-174	-141	-125	114
	E	5°C	29	73	84	87	89	90	91	91
		25°C	36	50	57	60	62	64	65	66
		40°C	67	65	66	66	68	69	70	71
	J	5°C	71	69	70	70	72	73	73	74
		25°C	72	43	31	30	34	40	45	48
		40°C	-711	-181	-87	-70	-63	-67	-73	-80
SM-9.5E	C	5°C	75	80	81	81	81	81	81	81
		25°C	33	73	80	80	80	78	76	75
		40°C	30	46	55	59	63	66	68	69
SM-12.5D	A	5°C	53	42	38	37	38	39	40	41
		25°C	25	29	41	47	55	62	66	68
		40°C	-1854	-1154	-648	-468	-276	-166	-113	82
SMA-12.5	L	5°C	93	94	94	94	93	93	92	92
		25°C	90	93	93	93	92	91	90	90
		40°C	93	92	90	89	87	86	85	84

Fatigue Response Evaluation

Characteristic plots of fatigue life versus applied strain are described for each mixture using the form:

$$N_f = K_0 \varepsilon^{-K_1}$$

[Eq. 17]

where

N_f = fatigue life, cycles
ε = applied strain, mm/mm
K_0 and K_1 = regression coefficients.

It is reported that K_1 and K_2 are dependent on mixture properties (Irwin and Gallaway, 1974; Van Dijk and Visser, 1977); however, analysis of the mixtures used in this study could not determine the validity of property-based relationships. This may be due to the limited range of values found for the mixture properties. Details of the mixture properties are presented in

Appendix B. Table 17 summarizes the coefficients K_1 and K_2 for each Smart Road section and mixture. In this study, it was observed that a linear relationship exists between the values of K_1 and K_2; this relationship is illustrated in Figure 4.

Figure 5 demonstrates the expected average fatigue life for the five mixture types evaluated at the Smart Road under various applied strains. The expected fatigue life was determined using the average mixture values for K_1 and K_2 shown in Table 18; it should be noted that these are average values and include the variation in performance due to the different sample preparation methods (i.e., field-field and field-lab). Figure 5 indicates that the SMA mix (SMA-12.5) had the best expected fatigue life performance when compared to that of the other mixes. It is important to note that the benefits are present through a wide range of applied loading

Table 17. K_1 and K_2 Coefficients for Fatigue Characterization from Eq. 17

Mixture	Section	Preparation Method	K_1	K_2	R^2
SM-9.5A	D	Field-Lab	6.3663×10^{15}	4.1864	0.9816
		Lab-Lab	4.6947×10^{16}	4.6674	0.9855
		Design-Lab	2.4399×10^{17}	4.9437	0.9803
	I^a	Field-Lab	1.0897×10^{19}	5.5745	0.9895
		Lab-Lab	7.9752×10^{16}	4.8336	0.9906
		Design-Lab	2.0298×10^{16}	4.6670	0.9537
	Mixture Average Value		1.6879×10^{16}	4.5091	0.8762
SM-9.5D	B	Field-Lab	5.1367×10^{14}	3.8650	0.8393
		Lab-Lab	1.2424×10^{18}	5.2555	0.9791
		Design-Lab	4.0147×10^{18}	5.3580	0.9544
	E	Field-Lab	1.5047×10^{18}	5.2267	0.9752
	F	Field-Lab	3.5980×10^{18}	5.3073	0.9648
	G	Field-Lab	1.3658×10^{18}	5.2077	0.9160
	H	Field-Lab	7.2526×10^{17}	5.1073	0.9875
	E-H	Lab-Lab	1.5092×10^{18}	5.1814	0.9760
	J	Field-Lab	2.2568×10^{17}	5.0413	0.9598
		Lab-Lab	7.7762×10^{18}	5.5657	0.9890
	Mixture Average Value		2.5496×10^{17}	4.9340	0.9125
SM-9.5E	C	Field-Lab	3.5695×10^{22}	6.5922	0.9282
		Lab-Lab	1.3266×10^{15}	3.9916	0.9142
		Design-Lab	8.5437×10^{20}	6.1179	0.9395
		Field-Field (all specimens)	2.7098×10^{17}	4.4111	0.8291
	Mixture Average Value		2.9395×10^{15}	4.0866	0.7326
SM-12.5D	A	Field-Lab	1.3610×10^{19}	5.5561	0.9476
		Lab-Lab	1.5371×10^{18}	5.1980	0.9782
		Design-Lab	3.4735×10^{17}	4.9849	0.9798
	Mixture Average Value		2.0560×10^{18}	5.2648	0.9605
SMA-12.5	L	Field-Lab	1.6114×10^{22}	6.5740	0.8699
		Design-Lab	5.4777×10^{13}	3.3251	0.6920
	Mixture Average Value		1.6536×10^{16}	4.2674	0.6644

[a]Designed using high laboratory compaction.
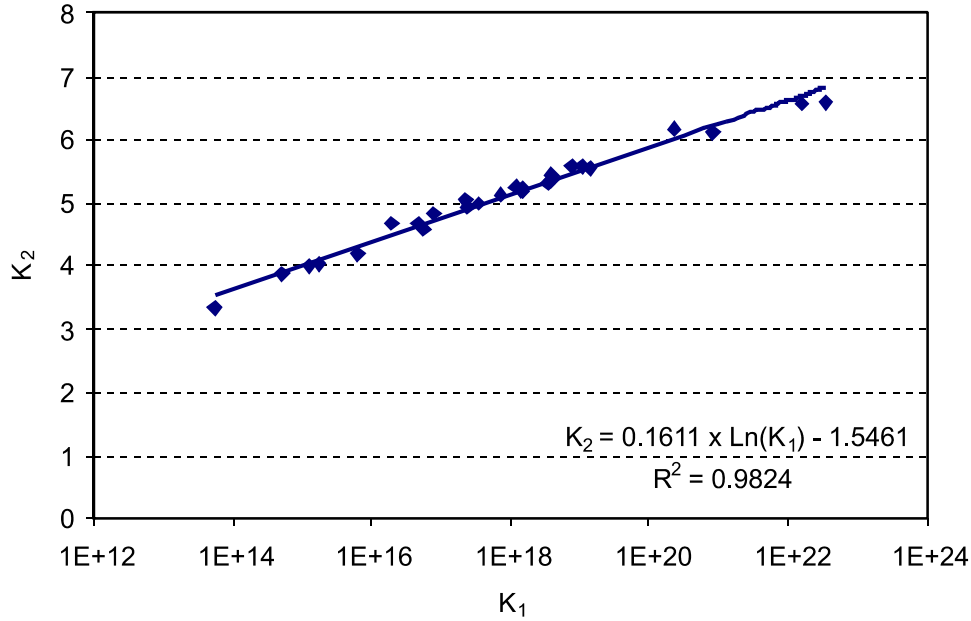
Figure 4. Relationship Between K_1 and K_2 in This Study

$$K_2 = 0.1611 \times \text{Ln}(K_1) - 1.5461$$
$$R^2 = 0.9824$$
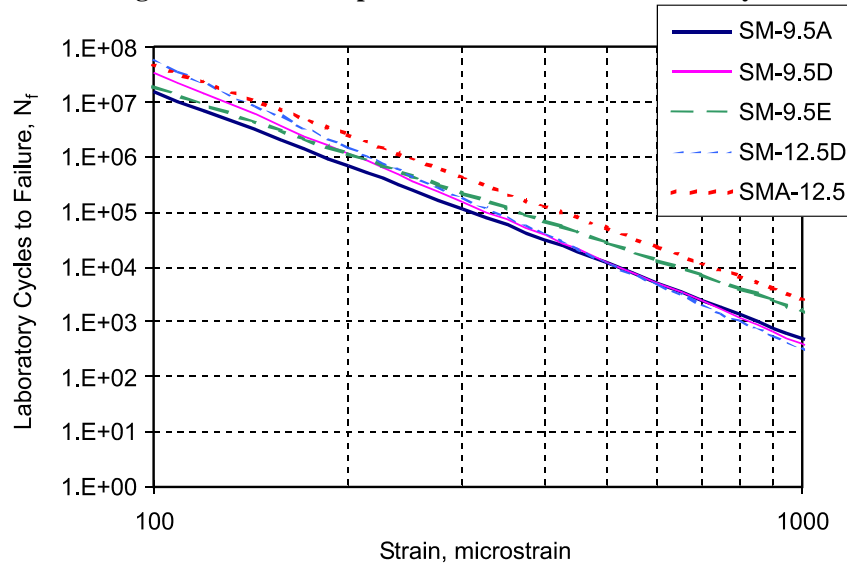
Figure 5. Expected Mixture Performance Based on Mixture Average K_0 and K_1 from Table 17

strains. Better performance is also predicted for the SM-9.5E mixture at applied strains above approximately 300 μstrain, indicating the potential benefits of the use of polymer-modified binders (SM-9.5E uses a modified PG 76-22 binder).

An alternative to the form expressed in Eq. 17, introduced by Monismith et al. (1985), that includes the mixture stiffness as a factor is:

$$N_f = K_0 \varepsilon^{-K_1} S_0^{-K_2}$$

[Eq. 18]

where

S_0 = initial mixture stiffness, Pa
K_2 = regression coefficient.

23

Table 18. Values of A and z for All Mixtures from Eq. 21

Mixture	Section	Preparation Method	A	z	R^2
SM-9.5A	D	Field-Lab	0.5169	0.5160	0.9757
		Lab-Lab	0.1357	0.5840	0.9874
		Design-Lab	0.1429	0.5806	0.9916
	I	Field-Lab	0.0950	0.6338	0.9925
		Lab-Lab	0.1374	0.5751	0.9901
		Design-Lab	0.0991	0.5801	0.9781
SM-9.5D	B	Field-Lab	0.0905	0.6263	0.9672
		Lab-Lab	0.0908	0.6228	0.9938
		Design-Lab	0.0854	0.6361	0.9871
	E	Field-Lab	0.0828	0.6414	0.9899
	F	Field-Lab	0.1404	0.6077	0.9801
	G	Field-Lab	0.0866	0.6409	0.9690
	H	Field-Lab	0.1154	0.6166	0.9918
	E-H	Lab-Lab	0.1349	0.6028	0.9874
	J	Field-Lab	0.0778	0.6178	0.9850
		Lab-Lab	0.0559	0.6562	0.9975
SM-9.5E	C	Field-Lab	0.1573	0.6150	0.9882
		Lab-Lab	0.2372	0.5467	0.8880
		Design-Lab	0.0407	0.7228	0.9834
		Field-Field (all specimens)	0.1095	0.6165	0.9072
SM-12.5D	A	Field-Lab	0.0465	0.6860	0.9716
		Lab-Lab	0.1127	0.6128	0.9929
		Design-Lab	0.1196	0.6059	0.9880
SMA-12.5	L	Field-Lab	0.0352	0.7507	0.9794
		Design-Lab	0.2038	0.5666	0.8796

It is thought that the quantities K_0, K_1, and K_2 are related to mixture properties; however, specific relations are not well supported in the literature. A preliminary evaluation of the use of Eq. 18 was performed; however, for 23 of the 31 sets of fatigue beams used in this study, the initial mixture stiffness was found to be statistically insignificant in fitting the model. Thus, verification of any potential relationships between K_0, K_1, and K_2 and mixture properties was not performed. In addition, Harvey and Tsai (1996) offered experimental results indicating that stiffness should not be included in models used for fatigue life evaluation, as conflicting results were found as to the effect of stiffness on fatigue life.

For viscoelastic materials, fatigue damage is related to the amount of energy dissipated in the specimen during testing. This relationship is suitable for asphalt mixtures as the dissipated energy can be used to explain the decrease in mechanical properties, such as flexural stiffness, during testing. Dissipated energy can be calculated by integrating the stress-strain hysteresis curve over one full cycle. The dissipated energy per unit volume per cycle is expressed as:

$$w_i = \pi \sigma_i \, \varepsilon_i \sin \phi_i \qquad \text{[Eq. 19]}$$

where

w_i = dissipated energy at load cycle i
σ_i = stress amplitude at load cycle i
ε_i = strain amplitude at load cycle i
ϕ_i = phase angle between stress and strain wave signals.

In addition, the accumulation of damage is evaluated by considering the total energy dissipated during loading. Thus, the total, or cumulative, dissipated energy is then determined as:

$$W_{fat} = \sum_{i=1}^{n} w_i$$

[Eq. 20]

where W_{fat} is the cumulative dissipated energy. The cumulative dissipated energy may be related to fatigue life as follows (Van Dijk, 1975):

$$W_{fat} = A \cdot \left(N_f\right)^z$$

[Eq. 21]

Characteristic plots of cumulative dissipated energy versus fatigue life are available from the author upon request. Table 18 summarizes the values of A and z for each mixture. Evaluation of these values indicates that there is a moderate relationship between A and z, as shown in Figure 6. Regression analysis to evaluate relationships between volumetric properties and the coefficients A and z showed no significant relationships; this is likely due to the limited range of volumetric quantities, as discussed previously.

Additional potential equations for the prediction of fatigue response that include cumulative dissipated energy were considered in this study:

$$N_f = K_0 \cdot \varepsilon^{K_1} \cdot CDE^{K_3}$$

[Eq. 22]
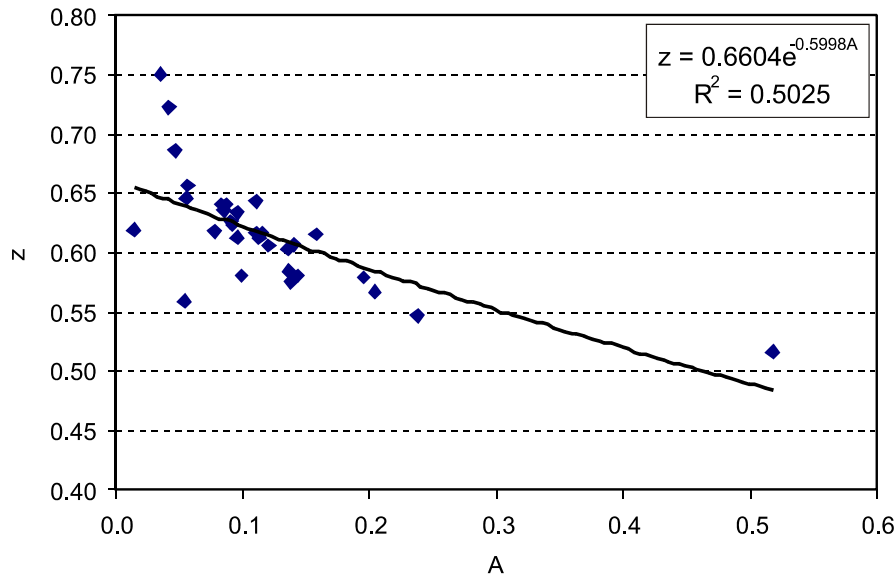
Figure 6. Relationship Between A and z from Table 18

where

CDE = cumulative dissipated energy at failure, kN-mm/ mm^3
K_3 = regression coefficient.

$$N_f = K_0 \cdot \varepsilon^{K_1} \cdot S_0^{K_2} \cdot CDE^{K_3}$$

[Eq. 23]

Details of the evaluation of these equations and their use in evaluating mixture performance are discussed in the following sections.

Fatigue Performance of Mixtures

The goals of this study included investigating the factors affecting mixture response to fatigue loading and comparatively evaluating mixture performance to identify better performing mixtures. The methods used to perform the comparative analyses included analysis of variance (ANOVA) and general linear modeling (GLM) techniques. These techniques require the assumption of normally distributed variables; however, Tayebali et al. (1994) reported that fatigue data are approximately log-normally distributed, and thus the log-transformed data may be used for analysis. The models considered were generally of a power nature; following the recommendation in the literature (Tayebali et al., 1994), log-transformations were applied. A convenient result of this transformation was the linearization of the proposed models presented previously, which enhanced the ease of analysis.

Evaluation included the consideration of significant regressors and evaluation of the coincidence of slopes and intercepts to determine the effectiveness of models for predicting fatigue response. Factors thought to have influence on fatigue performance included production practice (plant or laboratory procedures), compaction, test loading frequency, presence and duration of rest periods during loading, and in-situ location and orientation of the mixture.

Effects of Production Method

One focal point of this study was the evaluation of the effects on laboratory performance of asphalt mixtures attributable to the differences between field and laboratory production practices. Analyses of combinations of production methods were performed to assess these effects. A coincidence of slopes and intercepts methodology was used initially for analysis as it can identify data sets for which fitted models are statistically identical. A summary of the results obtained by evaluating the differences between the K_0 and K_1 terms previously presented in Table 17 is shown in Table 19. It should be noted that either a slope or intercept can be significantly different, leading to the conclusion that the treatments (in this case, production method) may have a significant effect on response, generally causing either a shift in response (significantly different intercepts) or a change in behavioral pattern (significantly different slopes).

Table 19. Results of Analysis Comparing Production Effects Using Coincidence of Slopes and Intercepts

Mixture	Section	Intercept	Contrast	DL	FL	Slope	Contrast	DL	FL
SM-9.5A	D	K_0	FL	NS	-	K_1	FL	sig	-
			LL	sig	NS		LL	NS	NS
	I[a]	K_0	FL	sig	-	K_1	FL	NS	-
			LL	NS	sig		LL	NS	NS
SM-9.5D	B	K_0	FL	sig	-	K_1	FL	sig	-
			LL	NS	NS		LL	NS	sig
	E	K_0	FL	NS	-	K_1	FL	NS	-
			LL	NS	NS		LL	NS	NS
	F	K_0	FL	NS	-	K_1	FL	NS	-
			LL	NS	NS		LL	NS	NS
	G	K_0	FL	NS	-	K_1	FL	NS	-
			LL	NS	NS		LL	NS	NS
	H	K_0	FL	NS	-	K_1	FL	NS	-
			LL	NS	NS		LL	NS	NS
	J	K_0	FL	NS	-	K_1	FL	NS	-
			LL	NS	NS		LL	NS	NS
SM-9.5E	C	K_0	FL	NS	-	K_1	FL	NS	-
			LL	sig	sig		LL	sig	sig
SM-12.5A	A	K_0	FL	NS	-	K_1	FL	NS	-
			LL	NS	sig		LL	NS	NS
SMA-12.5	L	K_0	FL	sig	-	K_1	FL	sig	-

Effects of Plant and Laboratory Production

The differences between field-lab and lab-lab fatigue specimens were evaluated to investigate the effects of plant production processes as compared to laboratory production processes. From Table 19, it can be seen that the values of both K_0 and K_1 were statistically different only for the SM-9.5E mixture in section C. The volumetric properties of both mixtures, shown in Table 17, do not indicate a reason for the difference in performance. The SM-9.5A and SM-12.5A mixtures (from sections I and A, respectively) were associated with significant differences in the value of the intercept coefficient, K_1. This indicates that the mixtures had similar trends in reduction of fatigue life under increasing strains, although there is a shift in the strain-life relationship attributable to the production method. In both cases, the expected fatigue life of the field-lab mixture was higher than that of the lab-lab mixture; this was likely due to the differences in the air voids contents with the two production methods, with the field-lab mixtures having lower air void contents, as shown in Table 20. The SM-9.5D mixture in section B was associated with a significant difference in the value of K_2, the slope coefficient, and different responses at differing strains. As shown in Figure 7, at applied strains below 300 µstrain, the lab-lab mixture is expected to have improved fatigue performance, whereas at strains greater than 300 µstrain the field-lab mixture is expected to have a greater fatigue life. The cause of the difference in performance of the SM-9.5D field-lab and lab-lab mixtures is not obvious, as the volumetric properties were found to be similar between the two production methods.

27

Table 20. Average Volumetric Values for Field-Lab and Lab-Lab Fatigue Specimens

Mix	Section	Asphalt (%)			VTM (%)		
		Field-Lab	Lab-Lab	Difference	Field-Lab	Lab-Lab	Difference
SM-9.5A	D	6.3	6.8	0.5	5.1	8.2	3.1
	I[a]	5.4	5.3	0.1	6.1	10.2	4.1
SM-9.5D	B	4.7	5.4	0.6	9.0	7.7	1.3
	E	5.9	6.0	0.1	7.2	8.2	1.0
	F	5.4		0.6	8.3		0.1
	G	6.3		0.3	8.8		0.6
	H	5.6		0.4	8.6		0.4
	J	4.9	5.1	0.2	11.3	10.5	0.8
SM-9.5E	C	5.8	6.0	0.2	7.3	8.9	1.6
SM-12.5D	A	5.9	5.9	0.0	7.6	11.2	3.6

[a]Designed using high laboratory compaction.
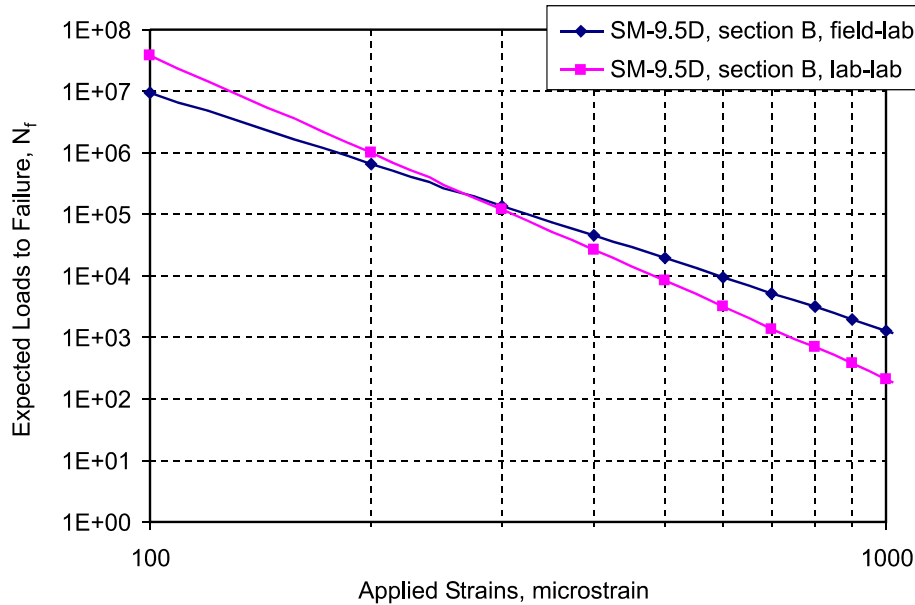
Figure 7. Expected Fatigue Performance of SM-9.5D, Section B

Effects of Production Mixture Differences

The differences in performance between lab-lab and design-lab mixtures are due to deviations in the produced mixture as compared to the mixture design. For this evaluation, both mixture types were produced in the laboratory to eliminate the additional variability found between field-lab mixtures and focus on the differences in mixture properties between the job mix formula and plant-produced material. Table 19 indicates that there is a significant difference in response as characterized by both K_1 and K_2 for the SM-9.5E mixture, whereas the SM-9.5A mixture in section D was associated with a significant difference only in the K_1 intercept. It is not obviously evident why the difference exists for the SM-9.5E mixture, as minimal differences

exist in volumetric properties between the two specimen sets, shown in Table 21. The source for the difference in K_1 seen in the SM-9.5A mixture is not evident as the difference in properties between the two specimen sets is again very small, as seen in Table 21. The findings for all other mixtures and sections indicate that the differences in as-produced material and the job-mix-produced material do not significantly affect the fatigue performance.

Differences between the field-lab and design-lab mixtures were evaluated to investigate the differences in fatigue performance between mixtures produced in the laboratory and at the plant from the job mix formula. From Table 19 it can be seen that the differences in both K_1 and K_2 are significant for the SM-9.5D mixture in section B and the SMA-12.5 mixture in section L. Consideration of the differences in asphalt and air void contents for the SM-9.5D mixture, shown in Table 22, does not indicate a clear cause for the difference in performance; however, the 5.0% difference in air void content in the SMA-12.5 mixture may influence the performance of the specimens.

Table 21. Average Volumetric Values for Design-Lab and Lab-Lab Fatigue Specimens

Mix	Section	Asphalt (%)			VTM (%)		
		Design-Lab	Lab-Lab	Difference	Design-Lab	Lab-Lab	Difference
SM-9.5A	D	6.3	6.8	0.5	7.9	8.2	0.3
	I[a]	5.4	5.3	0.1	10.8	10.2	0.6
SM-9.5D	B	5.3	5.4	0.1	9.6	7.7	1.9
	EFGH		6.0	0.7		8.2	1.4
	J		5.1	0.3		10.5	0.9
SM-9.5E	C	6.2	6.0	0.2	8.0	8.9	0.9
SM-12.5D	A	5.6	5.9	0.4	8.9	11.4	2.5

[a]Designed using high laboratory compaction.

Table 22. Average Volumetric Values for Field-Lab and Design-Lab Fatigue Specimens

Mix	Section	Asphalt (%)			VTM (%)		
		Field-Lab	Design-Lab	Difference	Field-Lab	Design-Lab	Difference
SM-9.5A	D	6.3	6.3	0.0	5.1	7.9	2.8
	I[a]	5.4	5.4	0.1	6.1	10.8	4.7
SM-9.5D	B	4.7	5.3	0.6	9.0	9.6	0.6
	E	5.9		0.5	7.2		2.4
	F	5.4		0.1	8.3		1.3
	G	6.3		1.0	8.8		0.8
	H	5.6		0.3	8.6		1.0
	J	4.9		0.4	11.3		1.7
SM-9.5E	C	5.8	6.2	0.4	7.3	8.0	0.7
SM-12.5D	A	5.9	5.6	0.3	7.6	8.9	1.3
SMA-12.5	L	6.8	6.3	0.5	5.9	10.9	5.0

[a]Designed using high laboratory compaction.

Table 19 also indicates that significant differences exist between the intercept coefficients, K_1, for the SM-9.5A mixtures in section I and between the slope coefficients, K_2, for the SM-9.5A mixtures in section D. Both mixtures show some differences in air void contents between the field-lab and design-lab specimens, with the difference being greatest for the section I SM-9.5A mixture; however, there is no evidence concerning why this factor may be affecting the intercept for one mixture and the slope for the other.

In summary, the data from this study show that differences in asphalt contents have a minimal impact on significant differences in fatigue performance, regardless of the production method or accuracy of production in replicating the job mix formula. Differences in the intercept coefficient, which may be considered similar to a low-strain fatigue limit, appear to be influenced by the air void content, which is expected and is well-documented in the literature; however, a clear trend in the minimum difference required for the air void content to affect the strain-life relationship significantly was not apparent.

The data from this study also show that the responses of mixes prepared using either laboratory or plant production methods do not differ significantly in terms of mixture fatigue performance. In addition, it was found that volumetric differences between the mixtures produced at the plant and those produced to match the job mix formula did not significantly influence the expected laboratory fatigue performance.

Effects of Compaction

One goal of this study was to evaluate the effect of compaction on the fatigue life of mixtures, including the differences between laboratory compaction of fatigue specimens and of specimens cut from the in-situ pavement. However, difficulties were encountered in the collection of the field specimens that might diminish the accuracy of this evaluation. Field specimens were cut from slabs removed from the pavement during installation of a weigh-in-motion facility. Unfortunately, the fatigue specimens were not collected from the slabs until approximately 1 year after the construction of the weigh-in-motion facility. This meant that the field specimens over-wintered as part of these separated slabs and were subjected to different weather than the in-place pavement; in addition, the slabs sustained some damage during removal that likely affected the fatigue response of the specimens. With these cautions, the following evaluation may be offered.

Comparisons between the production/compaction methods using Eq. 17 indicated that significant differences existed in the intercept coefficient for the field-lab and design-lab specimen sets when compared to the field-field specimens; this can be seen in Table 23. The differences between these mixtures may be influenced by air void content, as shown in Table 24, as the lab-lab and field-field specimen sets had similar average air void contents that were greater than those found for the field-lab and design-lab specimen sets. Figure 8 illustrates the expected fatigue performance of each mixture. It is interesting to note that although surface cracking was observed in the field-field specimens after slab removal from the pavement and before cutting into test specimens and it was assumed that they were damaged prior to testing, the field-field mixture is expected to perform better than all other mixtures at loading strains higher than approximately 250 μstrain.

Table 23. Results of Analysis Comparing Compaction Effects Using Coincidence of Slopes and Intercepts for SM-9.5 E, Section C, Mixtures

Intercept	Contrast	Field-Field	Slope	Contrast	Field-Field
K_0	Design-Lab	sig	K_1	Design-Lab	NS
	Field-Lab	sig		Field-Lab	NS
	Lab-Lab	NS		Lab-Lab	NS

Sig = significant, NS = not significant.

Table 24. Average Volumetric Values for SM-9.5E, Section C, Mixtures

Sample	Asphalt (%)	VTM (%)
Field-Field	5.8	8.6
Field-Lab	5.8	7.3
Lab-Lab	6.0	8.9
Design-Lab	6.2	8.0
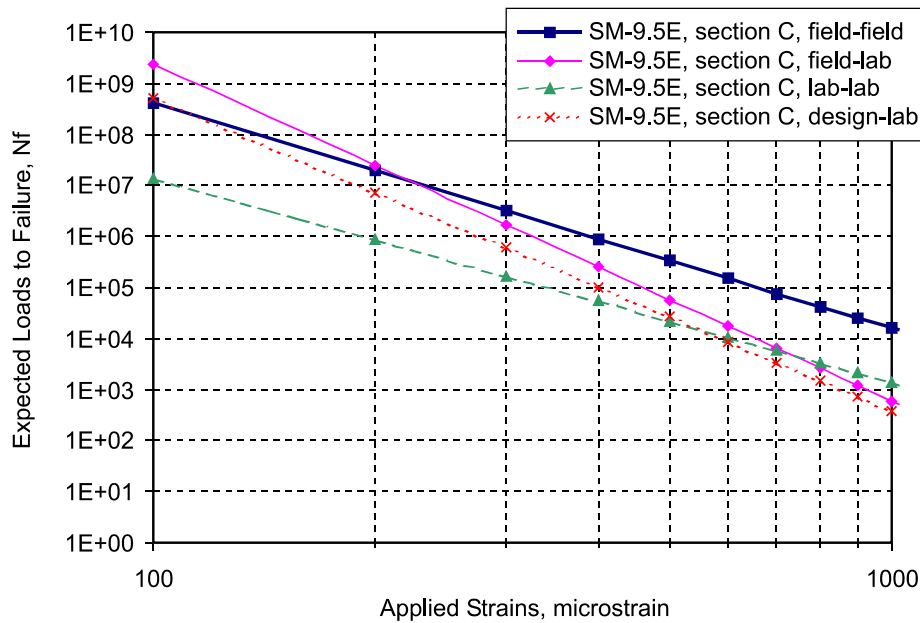
Figure 8. Expected Fatigue Performance: SM-9.5E, Section C

Effects of Loading Frequency

The effects of frequency of loading on fatigue life were evaluated as part of this study. Design-lab specimens of the SM-9.5E mixture were tested using loading frequencies of 1, 5, and 10 Hz. Results of testing were expressed in terms of applied stress and strain, stiffness, cumulative dissipated energy, and fatigue life.

An initial evaluation was performed to determine if correlations existed among test frequency, fatigue life, applied strain, cumulative dissipated energy, and initial stiffness. Significant correlations were found for several relationships using a sensitivity of $\alpha = 0.05$.

Applied strain was found to be highly correlated with cumulative dissipated energy; this was expected, since the dissipated energy is a function of the applied strain. This is presented graphically in Figure 9. A strong correlation was also seen between test frequency and initial stiffness. These relationships are further examined in the following paragraphs.

Regression analyses were performed to evaluate the trends in performance seen in the fatigue data; the results are presented in Table 25. The equations used for analysis were Eqs. 17, 18, 22, and 23. Eq. 17 is commonly accepted as a suitable relationship for fatigue. An investigation of the differences in the intercept term, denoted K_0, and the coefficient of the applied strain, denoted K_1, indicated that no trends were apparent for these terms with respect to frequency. Further statistical analysis of the equations indicated that no significant differences exist between the K_0 terms or between the K_1 terms. Thus, Eq. 17 can be used to predict fatigue life from applied strain without regard to the testing frequency. The relationship between fatigue life and applied strain is also presented in Figure 10, where the similarity in the relationship for all tested frequencies can be seen. This indicates that for the mixture tested, fatigue life is independent of the frequency of the applied strains.

Regarding the effects of frequency on the coefficients, clear trends can be seen for some coefficients. Increasing the testing frequency results in the following trends: the intercept term, K_0, increases; and the strain coefficient, K_1, decreases. There appears to be no clear relationship between frequency and the energy coefficient, K_2. Statistical analyses of the differences between frequencies for all coefficients indicated that changes in coefficients are not significant among the three test frequencies; resulting in the conclusion that one model is sufficient to capture the fatigue performance at test frequencies below 10 Hz. This finding contradicts previous evaluations by Monismith et al. (1961) and Deacon and Monismith (1967), which found that frequencies of 0.05 Hz to 0.3 Hz had no effect on fatigue life, although higher frequencies in the range of 0.5 Hz to 1.6 Hz decreased the fatigue life by approximately 20%. As the previous work was performed using lower frequencies and controlled stress testing, the possibility of different conclusions is unsurprising and results may also be complicated by the small sample set used for this evaluation.
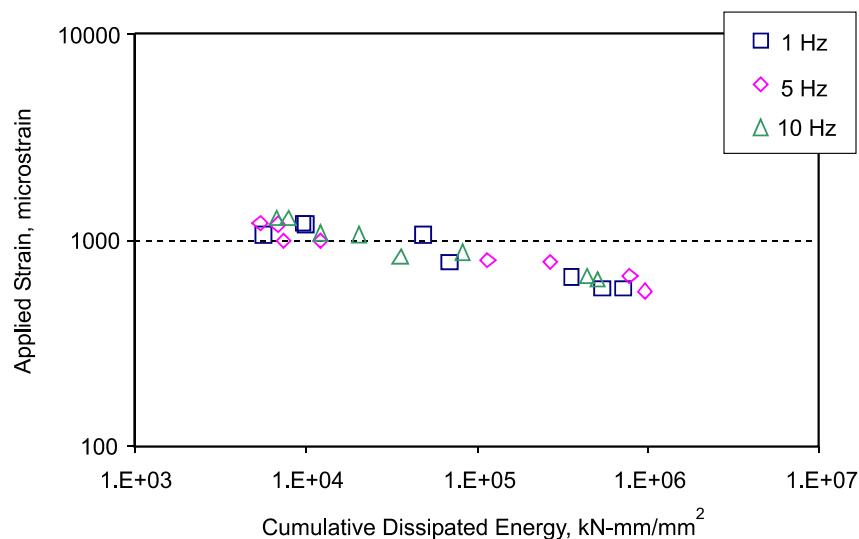
Figure 9. Applied Strain Versus Cumulative Dissipated Energy for Varying Load Frequencies

Table 25. Regression Results for Evaluation of Models

<table>
<tr><td colspan="7" align="center">$N_f = \beta_0 \times \varepsilon^{\beta_1}$ Eq. 17</td></tr>
<tr><td>Frequency</td><td>K_0</td><td>K_1</td><td>K_2</td><td>K_3</td><td>RMSE</td><td>adjusted R^2</td></tr>
<tr><td>1</td><td>50.791</td><td>-5.887</td><td>-</td><td>-</td><td>0.6642</td><td>0.8822</td></tr>
<tr><td>5</td><td>64.396</td><td>-7.901</td><td>-</td><td>-</td><td>0.6408</td><td>0.9162</td></tr>
<tr><td>10</td><td>52.438</td><td>-6.118</td><td>-</td><td>-</td><td>0.4528</td><td>0.9295</td></tr>
<tr><td>All</td><td>55.176</td><td>-6.531</td><td>-</td><td>-</td><td>0.5939</td><td>0.9006</td></tr>
<tr><td colspan="7" align="center">$N_f = \beta_0 \times \varepsilon^{\beta_1} \times S_0^{\beta_2}$ Eq. 18</td></tr>
<tr><td>Frequency</td><td>K_0</td><td>K_1</td><td>K_2</td><td>K_3</td><td>RMSE</td><td>adjusted R^2</td></tr>
<tr><td>1</td><td>75.740</td><td>-6.689</td><td>-2.7086</td><td>-</td><td>0.6575</td><td>0.8846</td></tr>
<tr><td>5</td><td>84.266</td><td>-7.443</td><td>-2.9232</td><td>-</td><td>0.5336</td><td>0.9419</td></tr>
<tr><td>10</td><td>16.604</td><td>-5.290</td><td>3.8171</td><td>-</td><td>0.4287</td><td>0.9368</td></tr>
<tr><td>All</td><td>56.702</td><td>-6.536</td><td>-0.1950</td><td>-</td><td>0.6038</td><td>0.8972</td></tr>
<tr><td colspan="7" align="center">$N_f = \beta_0 \times \varepsilon^{\beta_1} \times CDE^{\beta_3}$ Eq. 22</td></tr>
<tr><td>Frequency</td><td>K_0</td><td>K_1</td><td>K_2</td><td>K_3</td><td>RMSE</td><td>adjusted R^2</td></tr>
<tr><td>1</td><td>16.309</td><td>-1.445</td><td>-</td><td>1.053</td><td>0.0814</td><td>0.9982</td></tr>
<tr><td>5</td><td>16.816</td><td>-1.595</td><td>-</td><td>1.065</td><td>0.0980</td><td>0.9980</td></tr>
<tr><td>10</td><td>21.390</td><td>-2.187</td><td>-</td><td>0.931</td><td>0.0482</td><td>0.9992</td></tr>
<tr><td>All</td><td>23.697</td><td>-2.469</td><td>-</td><td>0.879</td><td>0.2373</td><td>0.9841</td></tr>
<tr><td colspan="7" align="center">$N_f = \beta_0 \times \varepsilon^{\beta_1} \times S_0^{\beta_2} \times CDE^{\beta_3}$ Eq. 23</td></tr>
<tr><td>Frequency</td><td>K_0</td><td>K_1</td><td>K_2</td><td>K_3</td><td>RMSE</td><td>adjusted R^2</td></tr>
<tr><td>1</td><td>23.531</td><td>-1.794</td><td>1.016</td><td>-0.652</td><td>0.0454</td><td>0.9995</td></tr>
<tr><td>5</td><td>25.856</td><td>-2.034</td><td>0.972</td><td>-0.718</td><td>0.0305</td><td>0.9998</td></tr>
<tr><td>10</td><td>26.453</td><td>-2.129</td><td>0.981</td><td>-0.719</td><td>0.0624</td><td>0.9996</td></tr>
<tr><td>All</td><td>25.207</td><td>-1.993</td><td>0.985</td><td>-0.680</td><td>0.0383</td><td>0.9996</td></tr>
</table>

Note: Shaded cells indicate variables that are not significant.
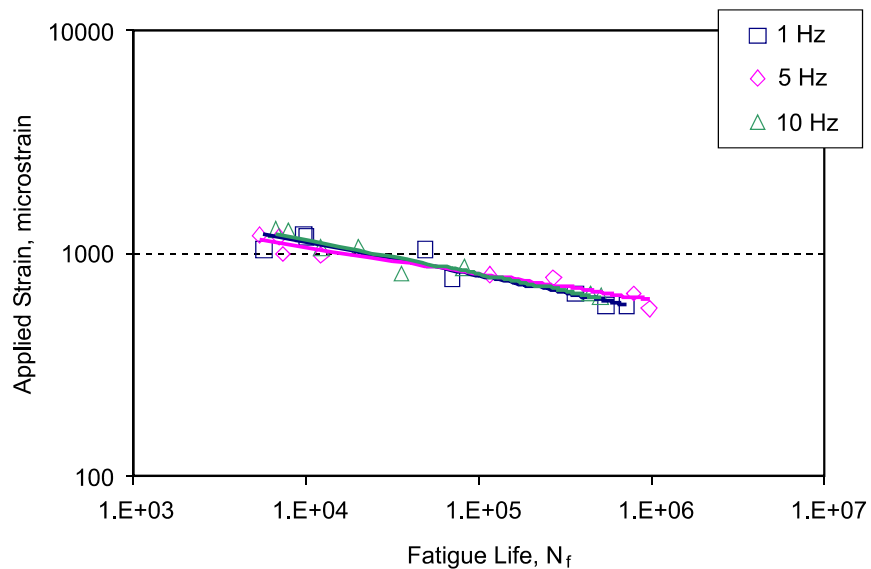
Figure 10.   Applied Strain Versus Fatigue Life for Varying Loading Frequencies

Eq. 23 was included in this analysis to investigate the combined effects of the cumulative dissipated energy and initial stiffness on the fatigue life prediction model. As can be seen in Table 25, the inclusion of both significantly lowered the RMSE values and increased the adjusted R^2 values over those of the other investigated models and did not render any of the coefficients insignificant. Trends with increasing test frequency may be seen in the K_0, K_1, and K_3 coefficients; however, it was again found that the differences in the coefficients attributable to differences in test frequency were not significant, so a single model may capture the fatigue performance at test frequencies of 10 Hz and below.

Effects of Rest Periods

The effects of rest periods during loading on fatigue life were evaluated as part of this study. Design-lab specimens of the SM-9.5E mixture were tested using 10 Hz sinusoidal loading with no rest period, a 0.4 sec rest period, or a 0.9 sec rest period following each load application. Test results were expressed in terms of applied stress and strain, stiffness, cumulative dissipated energy, and fatigue life.

An initial evaluation was performed to determine if correlations existed among test frequency, fatigue life, applied strain, cumulative dissipated energy, and initial stiffness. Correlation analyses indicated that significant correlations existed for several relationships using a sensitivity of $\alpha = 0.05$. Applied strain was highly correlated with cumulative dissipated energy, shown graphically in Figure 11. Correlations were also seen between initial stiffness and both rest period and cumulative dissipated energy, although these were not as strong.

Figure with equation $CDE = (2.8405 \times 10^{11}) \times \varepsilon^{-3.1713}$ and $R^2 = 0.7650$
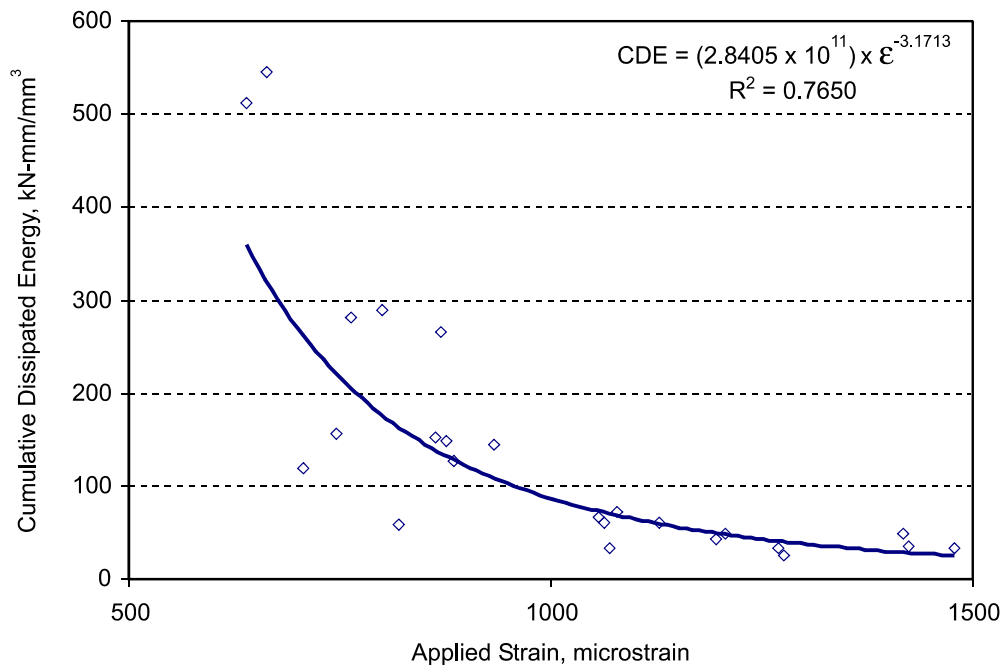
Figure 11.   Relationship Between Applied Strain and Cumulative Dissipated Energy Found for Frequency

Modeling of the fatigue performance is presented in Table 26, and an evaluation of the coincidence of slopes and intercepts is shown in Table 27. The first model considered, Eq. 17, is the relationship between applied strain and resulting fatigue life. Results of the evaluation did not indicate any trends in the values of the coefficients with respect to the length of the rest period. An investigation of the coincidence in the intercept and slope coefficients indicated that the regressed models used to describe the fatigue response with no rest period and with 0.9 sec rest periods were statistically similar, as no significant differences were observed between either the intercept or slope coefficients. However, significant differences were found between the regressed model with a 0.4 sec rest period and both models having no rest period and a 0.9 sec rest period. This is illustrated in Figure 12. It can be seen, however, that the model incorporating all testing data was not found to be significantly different from any rest period treatment and so may be used regardless of the rest period.

Table 26. Regression Results for Evaluation of Models

$N_f = K_0 \times \varepsilon^{K_1}$ Eq. 17						
Rest Period	K_0	K_1	K_2	K_3	RMSE	Adjusted R^2
None	5.9336E+22	6.1179	-	-	0.4528	0.9295
0.4 sec	1.1100E+16	3.7988	-	-	0.2694	0.9382
0.9 sec	2.1507E+21	5.5201	-	-	0.2733	0.9510
All tests	2.2079E+19	4.9046	-	-	0.5139	0.8483
$N_f = K_0 \times \varepsilon^{K_1} \times S_0^{K_2}$ Eq. 18						
Rest Period	K_0	K_1	K_2	K_3	RMSE	Adjusted R^2
None	1.6260E+07	5.2898	3.8171	-	0.4287	0.9368
0.4 sec	1.1367E+26	3.9766	-2.7304	-	0.2606	0.9421
0.9 sec	3.4320E+16	5.5668	1.4321	-	0.2685	0.9527
All tests	5.9410E+09	4.7136	2.6080	-	0.4856	0.8645
$N_f = K_0 \times \varepsilon^{K_1} \times CDE^{K_3}$ Eq. 22						
Rest Period	K_0	K_1	K_2	K_3	RMSE	Adjusted R^2
None	1.9473E+09	2.1865	-	0.9305	0.0482	0.9992
0.4 sec	8.5183E+08	1.9985	-	0.8879	0.0892	0.9932
0.9 sec	7.7392E+07	1.7241	-	1.0138	0.0564	0.9979
All tests	5.5493E+06	1.4160	-	1.1001	0.1530	0.9866
$N_f = K_0 \times \varepsilon^{K_1} \times S_0^{K_2} \times CDE^{K_3}$ Eq. 23						
Rest Period	K_0	K_1	K_2	K_3	RMSE	Adjusted R^2
None	3.0798E+11	2.1294	-0.7186	0.9809	0.0323	0.9996
0.4 sec	7.5494E+11	2.1329	-0.7088	0.8443	0.0926	0.9927
0.9 sec	2.5191E+07	1.8570	0.2766	0.9807	0.0574	0.9979
All tests	1.3113E+05	1.4710	0.5361	1.0704	0.1515	0.9868

Note: Shaded cells indicate that the regressor is not statistically significant.

Table 27.   Results of Analysis Comparing Effects of Rest Periods Using Coincidence of Slopes and Intercepts

$$N_f = K_0 \times \varepsilon^{K_1} \qquad Eq.\,17$$

Coefficient	Rest Period	All Tests	None	0.4 sec	Coefficient	Rest Period	All Tests	None	0.4 sec
K_0 intercept coefficient	None	NS	-	-	K_3 stiffness coefficient	None			
	0.4 sec	NS	sig	-		0.4 sec			
	0.9 sec	NS	NS	sig		0.9 sec			
K_1 strain coefficient	None	NS	-	-	K_4 CDE coefficient	None			
	0.4 sec	NS	sig	-		0.4 sec			
	0.9 sec	NS	ns	sig		0.9 sec			

$$N_f = K_0 \times \varepsilon^{K_1} \times CDE^{K_3} \qquad Eq.\,22$$

Coefficient	Rest Period	All Tests	None	0.4 sec	Coefficient	Rest Period	All Tests	None	0.4 sec
K_0 intercept coefficient	None	NS	-	-	K_3 stiffness coefficient	None			
	0.4 sec	NS	NS	-		0.4 sec			
	0.9 sec	NS	NS	NS		0.9 sec			
K_1 strain coefficient	None	NS	-	-	K_4 CDE coefficient	None	NS	-	-
	0.4 sec	NS	NS	-		0.4 sec	NS	NS	-
	0.9 sec	NS	NS	NS		0.9 sec	NS	NS	NS

Note: Shaded cells indicate that the regressor is not included in the model.
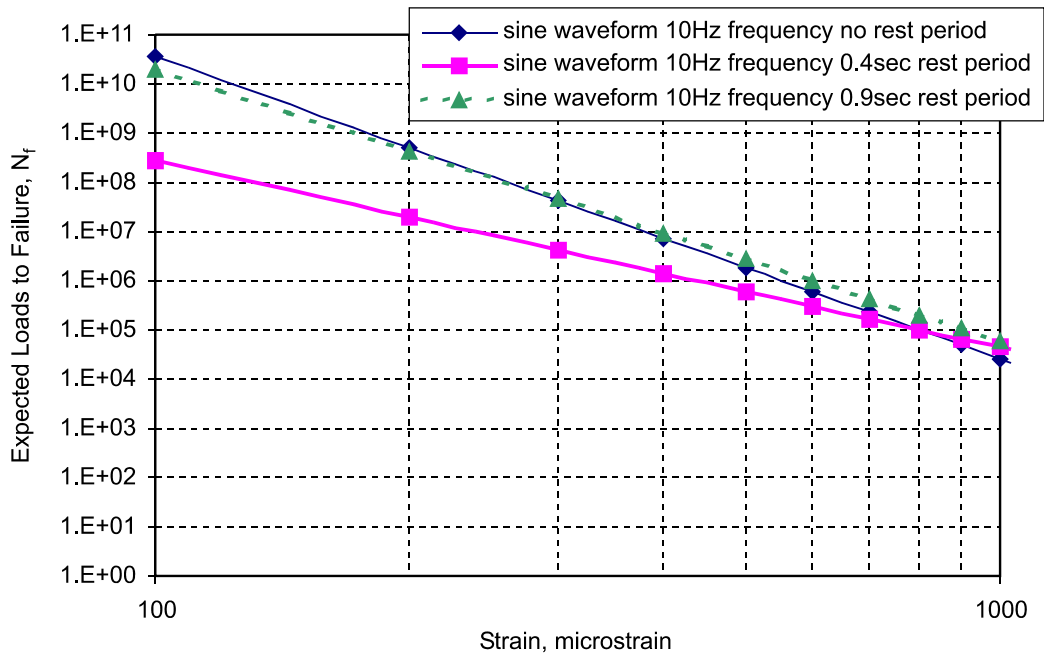
Figure 12. Expected Fatigue Response of SM-9.5E, Section C, Design-Lab Mixtures With Varying Rest Periods

The second model evaluated, Eq. 18, includes initial stiffness as a factor in addition to applied strain. It is evident that initial stiffness is superfluous to the model, as the stiffness coefficient is not statistically significant when included on the model. Because of this, further evaluation of this model was not pursued.

An evaluation of Eq. 22 indicated that the addition of cumulative dissipated energy to the strain model (Eq. 17) offers improvement, as the RMSE values were reduced and the correlation coefficient (adjusted R^2) was increased. This is interesting given the strong correlation between cumulative dissipated energy and applied strain, as it would be expected that either could be unnecessary since the other would capture the response mechanism. Table 26 indicates increasing trends in the values of the intercept (K_0) and strain (K_1) coefficients with increasing rest period, although no trend was seen for the K_3 coefficient. The trends for K_1 and K_2 apparently were not statistically significant, though, as Table 26 indicates there are no differences between the regressed models; thus, it appears that inclusion of either the 0.4 sec or 0.9 sec rest period has no effect on fatigue life when predicted from applied strain and cumulative dissipated energy.

Eq. 23 was also considered during this analysis, and it was found that initial stiffness was not significant when applied strain and cumulative dissipated energy were included in the model. Thus, no further consideration was given to the model.

Effects of Location within Pavement Surface

As part of this study, the effects of location and orientation of specimens cut from the wearing surface on fatigue life were evaluated. As previously noted, field specimens were cut from large slabs removed from the pavement during installation of a weigh-in-motion facility. The slabs were left unprotected over the winter following removal from the pavement and sustained some damage that may have affected the fatigue response of the specimens.

The SM-9.5E field specimens from section C were tested after being cut from the inner and outer wheelpaths and the center of the lane. Specimens cut with the longitudinal axis parallel with and perpendicular to the direction of traffic were compared with specimens cut from the outer wheelpath. Test results were expressed in terms of applied stress and strain, stiffness, cumulative dissipated energy, and fatigue life.

An evaluation was performed to determine if correlations existed between location in the pavement, fatigue life, applied strain, cumulative dissipated energy, and initial stiffness. Results showed significant correlations for several relationships using a sensitivity of $\alpha = 0.05$. Applied strain was highly correlated with cumulative dissipated energy, as expected, since dissipated energy is a function of applied strain. Correlations were also seen between location in pavement and both applied strain and initial stiffness.

Results of the regressions are presented in Table 28. The models were found to describe the observed data very well, as determined by the adjusted R^2 values. However, the results of the regressions using Eq. 18 indicated that the initial stiffness was not a significant contributor to the model when applied strain was used in the model. Interestingly, the initial stiffness was found to be a significant factor only for two specimen sets and the compilation of all sets when both applied strain and cumulative dissipated energy were included in the model. Thus, the models shown in Eqs. 18 and 23 were removed from analysis since they contained regressors that were not significant.

Table 28. Regression Results for Evaluation of Models at Locations Across Pavement

$N_f = K_0 \times \varepsilon^{K_1}$ Eq. 17						
Location	K_0	K_1	K_2	K_3	RMSE	Adjusted R^2
Center of lane-PP	1.3194E+18	4.5846	-	-	0.6239	0.8292
Outer wheelpath-PP	3.0677E+16	4.0459	-	-	0.6299	0.8749
Inner wheelpath-PP	1.6084E+22	6.1547	-	-	0.4853	0.9374
Inner wheelpath-PL	1.7162E+20	5.4374	-	-	0.5634	0.9138
All locations	2.7098E+17	4.4111	-	-	0.7384	0.8228

$N_f = K_0 \times \varepsilon^{K_1} \times S_0^{K_2}$ Eq. 18						
Location	K_0	K_1	K_2	K_3	RMSE	Adjusted R^2
Center of lane-PP	1.8736E+24	4.1056	2.2053	-	0.4630	0.9060
Outer wheelpath-PP	2.2266E+17	4.4130	0.1652	-	0.6893	0.8503
Inner wheelpath-PP	7.3176E+26	5.8729	1.6527	-	0.5220	0.9276
Inner wheelpath-PL	6.5892E+22	5.1417	1.0083	-	0.6138	0.8977
All locations	1.1638E+17	4.4124	0.1089	-	0.7520	0.8162

$N_f = K_0 \times \varepsilon^{K_1} \times CDE^{K_3}$ Eq. 22						
Location	K_0	K_1	K_2	K_3	RMSE	Adjusted R^2
Center of lane-PP	2.3437E+08	1.7958	-	1.1358	0.1566	0.9892
Outer wheelpath-PP	2.7894E+08	1.7563	-	0.9394	0.1841	0.9893
Inner wheelpath-PP	1.2093E+09	1.9812	-	1.0744	0.0720	0.9886
Inner wheelpath-PL	2.0316E+08	1.7644	-	1.1375	0.0503	0.9993
All locations	4.0866E+09	2.1382	-	0.9530	0.1883	0.9885

$N_f = K_0 \times \varepsilon^{K_1} \times S_0^{K_2} \times CDE^{K_3}$ Eq. 23						
Location	K_0	K_1	K_2	K_3	RMSE	Adjusted R^2
Center of lane-PP	1.2356E+12	2.0578	0.7906	0.9592	0.0586	0.9985
Outer wheelpath-PP	7.6904E+12	2.1720	0.9477	0.9975	0.0214	0.9999
Inner wheelpath-PP	2.0896E+11	1.9400	0.7056	1.0540	0.0412	0.9995
Inner wheelpath-PL	1.2841E+09	1.7704	0.2223	1.1155	0.0252	0.9998
All locations	3.0896E+11	1.9760	0.7141	1.0173	0.06984	0.9984

PP = perpendicular to traffic, PL = parallel with traffic.
Note: Shaded cells indicate that the regressor is not statistically significant.

The results from the regression analysis, with the exception of those for Eqs. 18 and 23, were used in the comparison of location and orientation within the pavement through the analysis of intercepts and slopes methodology. A summary of the results obtained by evaluating the differences among the K_0, K_1, K_3, and K_4 terms in each model considered is shown in Table 29.

The model expressed by Eq. 17 indicates significant differences in the slope and intercept coefficients for the inner and outer wheelpath specimens oriented perpendicular to the direction of traffic. This was likely influenced by the difference in the air void content between the two specimen sets, shown in Table 30, although is it not clear why the higher air void content of the inner wheelpath specimens oriented perpendicular to the direction of traffic (IWP-PP) would not also lead to significant differences when compared to the other specimen sets. In addition, significant differences were not found between any of the specimen sets and the summary model fitted from the combined data. This supports the observation seen in Figure 13 that performance

Table 29. Results of Analysis Comparing Location Effects Using Coincidence of Slopes and Intercepts

$$N_f = K_0 \times \varepsilon^{K_1} \qquad \text{Eq. 17}$$

Coefficient	Location	All	CL-PP	OWP-PP	IWP-PP	Coefficient	Location	All	CL-PP	OWP-PP	IWP-PP
K_0	CL-PP	NS	-	-	-	K_2	CL-PP				
	OWP-	NS	NS	-	-		OWP-				
	IWP-PP	NS	NS	sig	-		IWP-PP				
	IWP-PL	NS	NS	NS	NS		IWP-PL				
K_1	CL-PP	NS	-	-	-	K_3	CL-PP				
	OWP-	NS	NS	-	-		OWP-				
	IWP-PP	NS	NS	sig	-		IWP-PP				
	IWP-PL	NS	NS	NS	NS		IWP-PL				

$$N_f = K_0 \times \varepsilon^{K_1} \times CDE^{K_3} \qquad \text{Eq. 22}$$

Coefficient	Location	All	CL-PP	OWP-PP	IWP-PP	Coefficient	Location	All	CL-PP	OWP-PP	IWP-PP
K_0	CL-PP	NS	-	-	-	K_2	CL-PP				
	OWP-	NS	NS	-	-		OWP-				
	IWP-PP	NS	NS	NS	-		IWP-PP				
	IWP-PL	NS	NS	NS	NS		IWP-PL				
K_1	CL-PP	NS	-	-	-	K_3	CL-PP	NS	-	-	-
	OWP-	NS	NS	-	-		OWP-	NS	NS	-	-
	IWP-PP	NS	NS	NS	-		IWP-PP	NS	NS	NS	-
	IWP-PL	NS	NS	NS	NS		IWP-PL	NS	NS	NS	NS

CL-PP = center of lane perpendicular to traffic, OWP-PP = outer wheelpath perpendicular to traffic, IWP-PP = inner wheelpath perpendicular to traffic, IWP-PL = inner wheelpath parallel with traffic.

Note: Shaded cells indicate that the regressor is not included in the model.

Table 30. Average Asphalt and Air Void Contents for SM-9.5E, Section C, Specimens

Location	Asphalt (%)	VTM (%)
All	5.8	8.6
Center of lane-PP		7.4
Outer wheelpath-PP		7.5
Inner wheelpath-PP		12.9
Inner wheelpath-PL		6.8

PP = perpendicular to traffic, PL = parallel with traffic.

between the varying locations as predicted with Eq. 17 was relatively similar, despite the differences of the IWP-PP model.

Table 28 also provides the results of the regression using Eq. 22, and Table 29 includes a summary of the differences in coefficients. It can be seen that the addition of cumulative dissipated energy improves the model fit over that seen from Eq. 17. In addition, no significant differences between the coefficients were found attributable to location or orientation of the specimen sets. It was found that the summary model was sufficient to use for this modeling process, as no significant differences were found for coefficients between it and any of the location/orientation-differentiated models.
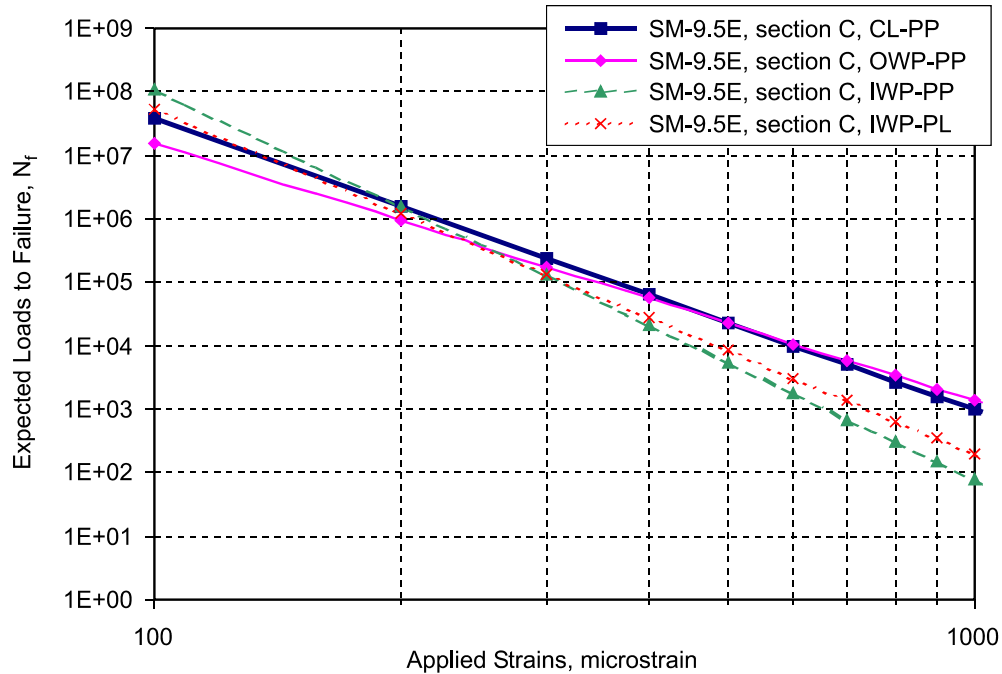
Figure 13. Comparison of Expected Fatigue Response, Modeled by Eq. 17, for SM-9.5E, Section C, Specimen Sets With Varying Locations and Orientations

In summary, fatigue response of evaluated mixtures was used to evaluate the effects on laboratory fatigue life of production and compaction methods, laboratory loading frequency, and presence or absence of rest periods during loading. In addition, field specimens were used to consider the influence of location within the lane on performance. Sufficient ranges in volumetric properties were not available to identify correlations between volumetric properties and laboratory fatigue performance conclusively, but differences in production and compaction methods were addressed.

CONCLUSIONS

- The results and conclusions of this study are applicable only to the surface mixtures tested and cannot be generalized to other VDOT or Superpave mixtures without verification testing.

- The viscoelasticity-based calculation for determination of creep compliance from deformation measurements proposed by Kim et al. (2002) is appropriate for determination of creep compliance.

- The regression and mechanistic creep compliance response models examined were unsuccessful in modeling the creep responses analyzed during this study.

- Differences in creep compliance response from the differing diameter specimen sets are likely a result of specimen and test variability, since the calculation of creep compliance from deformations is weighted to account for specimen diameter and height.

- Evaluations of the effects of laboratory and plant production and laboratory and field compaction were inconclusive. Differences in the asphalt content and air void content among the specimen sets may be contributing to the inconsistent comparisons seen in the data, but it is more likely that material variability is simply greater than production or compaction variability for the mixtures and materials used in this study.

- Simple regression models are satisfactory for the development of fatigue prediction models, although test data are necessary for calibration to particular mixture types.

- There is no relationship between fatigue model coefficients and the volumetric properties of the mixtures tested. This was likely due to the limited range of volumetric properties in the evaluated mixtures.

- Variability in volumetric properties encountered between the mixtures produced at the plant and those produced to match the job mix formula did not significantly influence the expected laboratory fatigue performance.

- Laboratory-compacted fatigue specimens have similar laboratory fatigue lives as compared to specimens cut from the pavement; differences observed in performance were due to differing air void contents.

- Predicted fatigue life is statistically independent of the frequency of the applied loads for the mixtures and frequencies used in this study.

- Predicted fatigue life is statistically independent of the presence of rest periods for the mixtures and rest period durations used in this study.

- Although void content appears to vary considerably with location in the pavement, the differences between fatigue life predictions for field-field specimens cut from different locations in the pavement are minimal.

RECOMMENDATIONS

1. *Testing was performed on variations of six Superpave mixtures having specific properties and placed at the Smart Road. The Virginia Transportation Research Council (VTRC) should perform testing on similar designated mixtures produced at the current time to verify the continuity of conclusions drawn from this study.* In addition, testing to provide direct input variables for the proposed *Mechanistic-Empirical Pavement Design Guide* should be performed to provide data for use in evaluating the Guide.

2. *VTRC should verify the correct test method for use in creep analysis as related to rutting.* Alternative methods include uniaxial creep testing with static or dynamic loading, rut testing, and wheel testing. In addition, if indirect tensile testing is used, adjustments to testing and

analysis procedures should be investigated to improve the variability of the test and difficulty of the analysis.

3. *For fatigue evaluation, VTRC should conduct additional testing on samples cut from the in-situ pavement to verify the results in this study regarding specimen orientation and in-situ mixture variability.* Fatigue evaluation of mixtures at different temperatures should be performed to characterize and quantify the temperature susceptibility of these mixtures under fatigue loading. Testing should also be performed on the asphalt base mixtures to evaluate their fatigue properties and contributions to the overall pavement fatigue response, as the base mixtures are even more important to consider in the occurrence of bottom-up cracking. Finally, the presented fatigue life models should be applied to pavement designs by comparing the fatigue response from the laboratory testing with observed fatigue development in in-situ pavements. This should result in a quantifiable response model to explain the discrepancies seen between laboratory fatigue and in-situ pavement fatigue. Empirical shift factors to account for differences have been introduced by several researchers (Majidzadeh et al., 1973; Monismith, 1981; Tseng and Lytton, 1990; Van Dijk, 1975) and range in value from approximately 0.95 to 20 to account for the differences; however, the accuracy of such factors depends on the availability of field data for calibration and verification.

COSTS AND BENEFITS ASSESSMENT

This study contributes to the understanding of the factors involved in creep and fatigue performance of asphalt mixtures. The mixture responses characterized by this study are related to the rutting and fatigue performance of asphalt pavements. The choice of appropriate asphalt materials to resist rutting and fatigue deterioration will result in reduced maintenance needs and longer service lives for pavements. The elimination of only 10,000 tons of material found to be susceptible to premature deterioration could potentially save VDOT approximately $350,000 annually by reducing the resurfacing needs. As this is merely a fraction of the approximately 3.5 million tons of asphalt placed annually in Virginia, further gains in the understanding of rutting and fatigue processes and prevention of premature deterioration have great potential payoff over the long term.

ACKNOWLEDGMENTS

REFERENCES

Buttlar, W.G., and R. Roque. (1994). Development and Evaluation of the Strategic Highway Research Program Measurement and Analysis System for Indirect Tensile Testing at Low Temperatures. In *Transportation Research Record 1454.* Transportation Research Board, Washington, DC, pp. 163-171.

Buttlar, W.G., R. Roque, and B. Reid. (1998). Automated Procedure for Generation of Creep Compliance Master Curve for Asphalt Mixtures. In *Transportation Research Record 1630.* Transportation Research Board, Washington, DC, pp. 28-36.

Button, J.W., D.N. Little, V. Jagadam, and O.J. Pendleton. (1994). Correlation of Selected Laboratory Compaction Methods with Field Compaction. In *Transportation Research Record 1454.* Transportation Research Board, Washington, DC, pp. 193-201.

Carpenter, S.H, K.A. Ghuzlan, and S. Shen. (2003). A Fatigue Endurance Limit for Highway and Airport Pavements. In *Transportation Research Record 1832.* Transportation Research Board, Washington, DC, pp. 131-138.

Christensen, D. (1998). Analysis of Creep Data from Indirect Tension Test on Asphalt Concrete. *Journal of the Association of Asphalt Paving Technologists,* Vol. 67, pp. 458-492.

Christensen, D., and D. Anderson. (1992). Interpretation of Dynamic Mechanical Test Data for Paving Grade Asphalts. *Journal of the Association of Asphalt Paving Technologists,* Vol. 61, pp. 67-116.

Consuegra, A., D.N. Little, H. Von Quintus, and J. Burati. (1989). Comparative Evaluation of Laboratory Compaction Devices Based on Their Ability to Produce Mixtures with Engineering Properties Similar to Those Produced in the Field. In *Transportation Research Record 1228.* Transportation Research Board, Washington, DC, pp. 80-87.

Deacon, J.A., and C.L. Monismith. (1967). Laboratory Flexural-Fatigue Testing of Asphalt-Concrete with Emphasis on Compound-Loading Tests. In *Highway Research Record 158,* Highway Research Board, Washington, DC, pp. 1-31.

Harvey, J.T., and B. Tsai. (1996). Effects of Asphalt Content and Air Void Content on Mix Fatigue and Stiffness. In *Transportation Research Record 1543.* Transportation Research Board, Washington, DC, pp. 38-45.

Harvey, J.T., and C.L. Monismith. (1993). Effects of Laboratory Asphalt Concrete Specimen Preparation Variables on Fatigue and Permanent Deformation Test Results Using Strategic Highway Research Program A-003A Proposed Testing Equipment. In *Transportation Research Record 1417.* Transportation Research Board, Washington, DC, pp. 38-48.

Irwin, L.H., and B.M. Gallaway. (1974). *Influence of Laboratory Test Method on Fatigue Test Results for Asphaltic Concrete.* ASTM Special Technical Publication 561. American Society for Testing and Materials, Philadelphia, pp. 12-46.

Khan, Z.A., H.I. Al-Abdul, I. Asi, and R. Ramadhan. (1998). Comparative Study of Asphalt Concrete Laboratory Compaction Methods to Simulate Field Compaction. *Construction and Building Materials,* Vol. 12, No. 6-7, pp. 373-384.

Kim, Y.R, J.S. Daniel, and H. Wen. (2002). *Fatigue Performance Evaluation of WesTrack Asphalt Mixtures Using Continuum Damage Approach.* Report No. FHWA/NC/2002-004. Federal Highway Administration, Washington, DC.

Majidzadeh, K., E. M. Kauffman, and C. W. Chang. (1973). *Verification of Fracture Mechanics Concepts to Predict Fatigue Cracking in Pavements.* Report No. FHWA-RD-73-91. Federal Highway Administration, Washington, DC.

Masad, E., S. Muhunthan, N. Shashidhar, and T. Harman. (1999). Quantifying Laboratory Compaction Effects on the Internal Structure of Asphalt Concrete. In *Transportation Research Record 1681.* Transportation Research Board, Washington, DC, pp. 179-185.

Monismith, C.L. (1981). Fatigue Characteristics of Asphalt Paving Mixtures and Their Use in Pavement Design. In *Proceedings of the 18th Paving Conference*, University of New Mexico, Albuquerque, pp. 1-43.

Monismith, C.L., J.A. Epps, and F.N. Finn. (1985). Improved Asphalt Mix Design. *Journal of the Association of Asphalt Paving Technologists,* Vol. 54, pp. 347-406.

Monismith, C.L., K.E. Secor, and E.W. Blackmer. (1961). Asphalt Mixture Behaviour in Repeated Flexure. *Journal of the Association of Asphalt Paving Technologists,* Vol. 30, pp. 188-222.

Roque, R., D.H. Hiltunen, W.G. Buttlar and T. Farwana. (1995). *Development of the SHRP Superpave Mixture Specification Test Method to Control Thermal Cracking Performance of Pavements.* ASTM Special Technical Publication 1265. American Society for Testing and Materials, Philadelphia, pp. 55-73.

Strategic Highway Research Program. (1994). *Fatigue Response of Asphalt-Aggregate Mixes.* Report SHRP-A-404. National Research Council, Washington, DC.

Tayebali, A., J. Deacon, J. Coplantz, J. Harvey, and C. Monismith. (1994). Mixture and Mode-of-Loading Effects on Fatigue Response of Asphalt-Aggregate Mixtures. *Journal of the Association of Asphalt Paving Technologists,* Vol. 63, pp. 118-151.

Tseng, K. H. and R. L. Lytton. (1990). Fatigue Damage Properties of Asphaltic Concrete Pavements. In *Transportation Research Record 1286,* Transportation Research Board, Washington, DC, pp. 84-97.

Van Dijk, W. (1975). Practical Fatigue Characterization of Bituminous Mixes. In *Proceedings of the Association of Asphalt Paving Technologists,* Vol. 44, pp. 38-74.

Van Dijk, W., and W. Visser. (1977). The Energy Approach to Fatigue for Pavement Design. In *Proceedings of the Association of Asphalt Paving Technologists,* Vol. 46, pp. 1-40.

Wen, H., and Y.R. Kim. (2002). Simple Performance Test for Fatigue Cracking and Validation with WesTrack Mixtures. In *Transportation Research Record 1789.* Transportation Research Board, Washington, DC, pp. 66-72.

APPENDIX A

MIXTURE DESIGNS

Table A1. Mixture Designs for SM-9.5A, Section D

Design-Lab		
Aggregate		
No. 8 Quartzite	Salem Stone Co., Sylvatus, Va.	50%
No. 10 Quartzite	Salem Stone Co., Sylvatus, Va.	30%
Concrete Sand	Wythe Stone Co., Wytheville, Va.	10%
Fine RAP	Adams Construction Co., Blacksburg, Va.	10%
Binder		
PG 64-22	Associated Asphalt, Inc., Roanoke, Va.	5.6%
Lab-Lab		
Aggregate		
No. 8 Quartzite	Salem Stone Co., Sylvatus, Va.	50%
No. 10 Quartzite	Salem Stone Co., Sylvatus, Va.	30%
Concrete Sand	Wythe Stone Co., Wytheville, Va.	10%
Fine RAP	Adams Construction Co., Blacksburg, Va.	10%
Binder		
PG 64-22	Associated Asphalt, Inc., Roanoke, Va.	5.6%

Table A2. Mixture Designs for SM-9.5A, Section I

Design-Lab		
Aggregate		
No. 8 Quartzite	Salem Stone Co., Sylvatus, Va.	50%
No. 10 Quartzite	Salem Stone Co., Sylvatus, Va.	30%
Concrete Sand	Wythe Stone Co., Wytheville, Va.	10%
Fine RAP	Adams Construction Co., Blacksburg, Va.	10%
Binder		
PG 64-22	Associated Asphalt, Inc., Roanoke, Va.	4.8%
Lab-Lab		
Aggregate		
No. 8 Quartzite	Salem Stone Co., Sylvatus, Va.	50%
No. 10 Quartzite	Salem Stone Co., Sylvatus, Va.	30%
Concrete Sand	Wythe Stone Co., Wytheville, Va.	10%
Fine RAP	Adams Construction Co., Blacksburg, Va.	10%
Binder		
PG 64-22	Associated Asphalt, Inc., Roanoke, Va.	5.0%

Table A3. Mixture Designs for SM-9.5D, Section B

Design-Lab		
Aggregate		
No. 8 Quartzite	Salem Stone Co., Sylvatus, Va.	60%
No. 10 Limestone	ACCO Stone Co., Blacksburg, Va.	20%
Concrete Sand	Wythe Stone Co., Wytheville, Va.	10%
Fine RAP	Adams Construction Co., Blacksburg, Va.	10%
Binder		
PG 70-22	Associated Asphalt, Inc., Roanoke, Va.	5.6%
Lab-Lab		
Aggregate		
No. 8 Quartzite	Salem Stone Co., Sylvatus, Va.	36%
No. 10 Limestone	ACCO Stone Co., Blacksburg, Va.	20%
Concrete Sand	Wythe Stone Co., Wytheville, Va.	10%
No. 10 Quartzite	Salem Stone Co., Sylvatus, Va.	23%
No. 10 Quartzite (filler)	Salem Stone Co., Sylvatus, Va.	1%
Fine RAP	Adams Construction Co., Blacksburg, Va.	10%
Binder		
PG 70-22	Associated Asphalt, Inc., Roanoke, Va.	4.7%

Table A.4 Mixture Designs for SM-9.5D, Sections E, F, G, and H

Design-Lab		
Aggregate		
No. 8 Quartzite	Salem Stone Co., Sylvatus, Va.	60%
No. 10 Limestone	ACCO Stone Co., Blacksburg, Va.	20%
Concrete Sand	Wythe Stone Co., Wytheville, Va.	10%
Fine RAP	Adams Construction Co., Blacksburg, Va.	10%
Binder		
PG 70-22	Associated Asphalt, Inc., Roanoke, Va.	5.4%
Lab-Lab		
Aggregate		
No. 8 Quartzite	Salem Stone Co., Sylvatus, Va.	48%
No. 10 Quartzite	Salem Stone Co., Sylvatus, Va.	12%
No. 10 Limestone	ACCO Stone Co., Blacksburg, Va.	20%
Concrete Sand	Wythe Stone Co., Wytheville, Va.	10%
Fine RAP	Adams Construction Co., Blacksburg, Va.	10%
Binder		
PG 70-22	Associated Asphalt, Inc., Roanoke, Va.	5.8%

Table A5. Mixture Design for SM-9.5D, Section J, Lab-Lab

Aggregate		
No. 8 Quartzite	Salem Stone Co., Sylvatus, Va.	48%
No. 10 Quartzite	Salem Stone Co., Sylvatus, Va.	12%
No. 10 Limestone	ACCO Stone Co., Blacksburg, Va.	20%
Concrete Sand	Wythe Stone Co., Wytheville, Va.	10%
Fine RAP	Adams Construction Co., Blacksburg, Va.	10%
Binder		
PG 70-22	Associated Asphalt, Inc., Roanoke, Va.	4.9%

Table A6. Mixture Designs for SM-9.5E, Section C

Design-Lab		
Aggregate		
No. 8 Quartzite	Salem Stone Co., Sylvatus, Va.	54%
No. 10 Quartzite	Salem Stone Co., Sylvatus, Va.	21%
Concrete Sand	Wythe Stone Co., Wytheville, Va.	10%
Fine RAP	Adams Construction Co., Blacksburg, Va.	15%
Binder		
PG 76-22	Koch Materials Co., Pennsauken, N.J.	5.8%
Lab-Lab		
Aggregate		
No. 8 Quartzite	Salem Stone Co., Sylvatus, Va.	52%
No. 10 Quartzite	Salem Stone Co., Sylvatus, Va.	23%
Concrete Sand	Wythe Stone Co., Wytheville, Va.	10%
Fine RAP	Adams Construction Co., Blacksburg, Va.	15%
Binder		
PG 76-22	Koch Materials Co., Pennsauken, N.J.	5.8%

Table A7. Mixture Designs for SM-12.5D, Section A

Design-Lab		
Aggregate		
No. 78 Quartzite	Salem Stone Co., Sylvatus, Va.	15%
No. 8 Quartzite	Salem Stone Co., Sylvatus, Va.	30%
No. 9 Quartzite	Salem Stone Co., Sylvatus, Va.	10%
No. 10 Limestone	Sisson and Ryan Quarry, Shawsville, Va.	20%
Sand	Castle Sand Co., New Castle, Va.	10%
Fine RAP	Adams Construction Co., Blacksburg, Va.	15%
Binder		
PG 70-22	Associated Asphalt, Inc., Roanoke, Va.	5.6%
Lab-Lab		
Aggregate		
No. 78 Quartzite	Salem Stone Co., Sylvatus, Va.	5%
No. 8 Quartzite	Salem Stone Co., Sylvatus, Va.	30%
No. 9 Quartzite	Salem Stone Co., Sylvatus, Va.	20%
No. 10 Limestone	Sisson and Ryan Quarry, Shawsville, Va.	20%
Sand	Castle Sand Co., New Castle, Va.	10%
Fine RAP	Adams Construction Co., Blacksburg, Va.	15%
Binder		
PG 70-22	Associated Asphalt, Inc., Roanoke, Va.	5.9%

Table A8. Mixture Designs for SM-12.5A, Section L

Design-Lab		
Aggregate		
No. 68 Quartzite	Salem Stone Co., Sylvatus, Va.	26%
No. 8 Quartzite	Salem Stone Co., Sylvatus, Va.	55%
No. 10 Quartzite	Salem Stone Co., Sylvatus, Va.	10%
Lime Filler	James River Lime, Buchanan, Va.	9%
Binder		
PG 76-22	Koch Materials Co., Pennsauken, N.J.	7.2%
Fiber		
Cellulose	Hi-Tech Asphalt Solutions, Mechanicsville, Va.	0.3%
Lab-Lab		
Aggregate		
No. 68 Quartzite	Salem Stone Co., Sylvatus, Va.	8%
No. 8 Quartzite	Salem Stone Co., Sylvatus, Va.	71%
No. 10 Quartzite	Salem Stone Co., Sylvatus, Va.	12%
Lime Filler	James River Lime, Buchanan, Va.	9%
Binder		
PG 76-22	Koch Materials Co., Pennsauken, N.J.	6.8%
Fiber		
Cellulose	Hi-Tech Asphalt Solutions, Mechanicsville, Va.	0.3%
Note: Aggregate and binder percentages are by weight of mixture. Fiber percentages are by weight of binder.		

APPENDIX B

MIXTURE VOLUMETRIC PROPERTIES

Table B1. Volumetric Properties for SM-9.5A Mixtures, Section D

Property	Field-Field	Field-Lab	Lab-Lab	Design-Lab
% Asphalt	6.29	6.29	6.76	6.25
G_{mm}	2.440	2.440	2.455	2.468
G_{mb}	2.393	2.408	2.434	2.379
G_b	1.03	1.03	1.03	1.03
G_{se}	2.687	2.687	2.729	2.722
G_{sb}	2.653	2.653	2.695	2.688
CF	0.034	0.034	0.034	0.034
Bulk Density	149.4	150.3	151.9	148.4
Density at N_{ini}	-	138.9	140.4	135.8
% passing No. 200	9.20	9.20	5.72	6.26

Table B2. VDOT Volumetric Specifications for SM-9.5D Mixtures, Section D

Property	Specification Min.	Max.	Field-Field		Field-Lab		Lab-Lab		Design-Lab	
VTM (%)	2.5	5.5	1.9	Fail	1.3	Fail	0.9	Fail	3.6	Pass
VMA (%)	12	-	15.5	Pass	14.9	Pass	15.8	Pass	17.0	Pass
VFA (%)	62	80	87.6	Fail	91.2	Fail	94.4	Fail	78.7	Pass
% Density at N_{ini}	-	89	-	-	91.2	Fail	91.6	Fail	88.1	Pass
F/A ratio	0.6	1.3	1.6	Fail	1.6	Fail	0.9	Pass	1.1	Pass

Table B3. Volumetric Properties for SM-9.5A Mixtures, Section I

Property	Field-Field	Field-Lab	Lab-Lab	Design-Lab
% Asphalt	5.42	5.42	5.31	5.37
G_{mm}	2.467	2.467	2.489	2.498
G_{mb}	2.440	2.429	2.340	2.390
G_b	1.03	1.03	1.03	1.03
G_{se}	2.681	2.681	2.704	2.718
G_{sb}	2.647	2.647	2.670	2.684
CF	0.034	0.034	0.034	0.034
Bulk Density	152.3	151.6	146.0	149.1
Density at N_{ini}	-	138.1	133.4	137.0
% passing No. 200	7.27	7.27	6.97	7.64

Table B4. VDOT Volumetric Specifications for SM-9.5A Mixtures, Section I

Property	Specification Min.	Specification Max.	Field-Field		Field-Lab		Lab-Lab		Design-Lab	
VTM (%)	2.5	5.5	1.1	Fail	1.5	Fail	6.0	Fail	4.3	Pass
VMA (%)	12	-	12.8	Pass	13.2	Pass	17.0	Pass	15.7	Pass
VFA (%)	62	80	91.6	Fail	88.5	Fail	64.8	Pass	72.5	Pass
% Density at N_{ini}	-	89	-	-	89.8	Fail	85.9	Pass	87.9	Pass
F/A ratio	0.6	1.3	1.5	Fail	1.5	Fail	1.4	Fail	1.6	Fail

Table B5. Volumetric Properties for SM-9.5D Mixtures, Section B

Property	Field-Field	Field-Lab	Lab-Lab	Design-Lab
% Asphalt	4.71	4.71	5.36	5.33
G_{mm}	2.450	2.450	2.513	2.494
G_{mb}	2.239	2.362	2.468	2.370
G_b	1.03	1.03	1.03	1.03
G_{se}	2.629	2.629	2.736	2.711
G_{sb}	2.574	2.574	2.681	2.656
CF	0.055	0.055	0.055	0.055
Bulk Density	139.7	147.4	154.0	147.9
Density at N_{ini}	-	135.1	141.7	133.1
% Passing No. 200	7.81	7.81	8.72	5.52

Table B6. VDOT Volumetric Specifications for SM-9.5D Mixtures, Section B

Property	Specification Min.	Specification Max.	Field-Field		Field-Lab		Lab-Lab		Design-Lab	
VTM (%)	2.5	5.5	8.6	Fail	3.6	Pass	1.8	Fail	5.0	Pass
VMA (%)	12	-	17.1	Pass	12.5	Pass	12.9	Pass	15.5	Pass
VFA (%)	62	80	49.7	Fail	71.6	Pass	86.0	Fail	68.0	Pass
% Density at N_{ini}	-	89	-	-	88.4	Pass	90.4	Fail	85.6	Pass
F/A ratio	0.6	1.3	2.0	Fail	2.0	Fail	1.9	Fail	1.2	Pass

Table B7. Volumetric Properties for SM-9.5D Mixtures, Section E

Property	Field-Field	Field-Lab	Lab – Lab (E, F, G, and H)
% Asphalt	5.85	5.85	6.00
G_{mm}	2.434	2.434	2.489
G_{mb}	2.317	2.400	2.442
G_b	1.03	1.03	1.03
G_{se}	2.659	2.659	2.737
G_{sb}	2.604	2.604	2.682
CF	0.055	0.055	0.055
Bulk Density	144.6	149.8	152.4
Density at N_{ini}	-	137.3	140.2
% passing No. 200	7.57	7.57	8.47

Table B8. VDOT Volumetric Specifications for SM-9.5D Mixtures, Section E

Property	Specification Min.	Specification Max.	Field-Field		Field-Lab		Lab – Lab (E, F, G, and H)	
VTM (%)	2.5	5.5	4.8	Pass	1.4	Fail	1.9	Fail
VMA (%)	12	-	16.2	Pass	13.2	Pass	14.4	Pass
VFA (%)	62	80	70.5	Pass	89.6	Fail	86.8	Fail
% Density at N_{ini}	-	89	-	-	90.4	Fail	90.2	Fail
F/A ratio	0.6	1.3	1.5	Fail	1.5	Fail	1.6	Fail

Table B9. Volumetric Properties for SM-9.5D Mixtures, Section F

Property	Field-Field	Field-Lab
% Asphalt	5.85	5.42
G_{mm}	2.434	2.502
G_{mb}	2.317	2.412
G_b	1.03	1.03
G_{se}	2.659	2.725
G_{sb}	2.604	2.670
CF	0.055	0.055
Bulk Density	144.6	150.5
Density at N_{ini}	-	137.5
% passing No. 200	7.57	6.88

Table B10. VDOT Volumetric Specifications for SM-9.5D Mixtures, Section F

Property	Specification Min.	Max.	Field-Field		Field-Lab	
VTM (%)	2.5	5.5	4.8	Pass	3.6	Pass
VMA (%)	12	-	16.2	Pass	14.5	Pass
VFA (%)	62	80	70.5	Pass	75.4	Pass
% Density at N_{ini}	-	89	-	-	88.1	Pass
F/A ratio	0.6	1.3	1.5	Fail	1.5	Fail

Table B11. Volumetric Properties for SM-9.5D Mixtures, Section G

Property	Field-Field	Field-Lab
% Asphalt	5.85	6.29
G_{mm}	2.434	2.499
G_{mb}	2.317	2.410
G_b	1.03	1.03
G_{se}	2.659	2.763
G_{sb}	2.604	2.708
CF	0.055	0.055
Bulk Density	144.6	150.4
Density at N_{ini}	-	137.6
% passing No. 200	7.57	8.35

Table B12. VDOT Volumetric Specifications for SM-9.5D Mixtures, Section G

Property	Specification Min.	Max.	Field-Field		Field-Lab	
VTM (%)	2.5	5.5	4.8	Pass	3.6	Pass
VMA (%)	12	-	16.2	Pass	16.6	Pass
VFA (%)	62	80	70.5	Pass	78.6	Pass
% Density at N_{ini}	-	89	-	-	88.2	Pass
F/A ratio	0.6	1.3	1.5	Fail	1.5	Fail

Table B13. Volumetric Properties for SM-9.5D Mixtures, Section H

Property	Field-Field	Field-Lab
% Asphalt	5.85	5.63
G_{mm}	2.434	2.507
G_{mb}	2.317	2.403
G_b	1.03	1.03
G_{se}	2.659	2.741
G_{sb}	2.604	2.686
CF	0.055	0.055
Bulk Density	144.6	149.9
Density at N_{ini}	-	137.4
% passing No. 200	7.57	7.57

Table B14. VDOT Volumetric Specifications for SM-9.5D Mixtures, Section H

Property	Specification Min.	Max.	Field-Field		Field-Lab	
VTM (%)	2.5	5.5	4.8	Pass	4.1	Pass
VMA (%)	12	-	16.2	Pass	15.6	Pass
VFA (%)	62	80	70.5	Pass	73.4	Pass
% Density at N_{ini}	-	89	-	-	87.8	Pass
F/A ratio	0.6	1.3	1.5	Fail	1.5	Fail

Table B15. Volumetric Properties for SM-9.5D Mixtures, Section J

Property	Field-Field	Field-Lab	Lab-Lab
% Asphalt	4.90	4.90	5.06
G_{mm}	2.518	2.518	2.524
G_{mb}	2.252	2.328	2.408
G_b	1.03	1.03	1.03
G_{se}	2.721	2.721	2.736
G_{sb}	2.666	2.666	2.681
CF	0.055	0.055	0.055
Bulk Density	140.5	145.3	150.2
Density at N_{ini}	-	133.0	137.6
% passing No. 200	6.31	6.31	6.72

Table B16. VDOT Volumetric Specifications for SM-9.5D Mixtures, Section J

Property	Specification Min.	Max.	Field-Field		Field-Lab		Lab-Lab	
VTM (%)	2.5	5.5	10.6	Fail	7.5	Fail	4.6	Pass
VMA (%)	12	-	19.7	Pass	16.9	Pass	14.7	Pass
VFA (%)	62	80	46.3	Fail	55.5	Fail	68.6	Pass
% Density at N_{ini}	-	89	-	-	84.6	Pass	87.3	Pass
F/A ratio	0.6	1.3	1.5	Fail	1.5	Fail	1.6	Fail

Table B17. Volumetric Properties for SM-9.5E Mixtures, Section C

Property	Field-Field	Field-Lab	Lab-Lab	Design-Lab
% Asphalt	5.80	5.80	6.02	6.16
G_{mm}	2.455	2.455	2.477	2.463
G_{mb}	2.309	2.399	2.426	2.431
G_b	1.03	1.03	1.03	1.03
G_{se}	2.684	2.684	2.721	2.711
G_{sb}	2.654	2.654	2.691	2.681
CF	0.03	0.03	0.03	0.03
Bulk Density	144.1	149.7	151.4	151.7
Density at N_{ini}	-	137.5	139.0	137.4
% Passing No. 200	8.18	8.03	7.56	6.60

Table B18. VDOT Volumetric Specifications for SM-12.5E Mixtures, Section C

Property	Specification Min.	Max.	Field-Field		Field-Lab		Lab-Lab		Design-Lab	
VTM (%)	2.5	5.5	6.0	Fail	2.3	Fail	2.0	Fail	1.3	Fail
VMA (%)	12	-	18.1	Pass	14.9	Pass	15.3	Pass	14.9	Pass
VFA (%)	62	80	67.0	Pass	84.6	Fail	86.6	Fail	91.4	Fail
% Density at N_{ini}	-	89	-	-	89.7	Fail	89.9	Fail	89.4	Fail
F/A ratio	0.6	1.3	1.5	Fail	1.5	Fail	1.3	Pass	1.1	Pass

Table B19. Volumetric Properties for SM-12.5D Mixtures, Section A

Property	Field-Field	Field-Lab	Lab-Lab	Design-Lab
% Asphalt	5.86	5.86	5.93	5.55
G_{mm}	2.422	2.422	2.510	2.497
G_{mb}	2.282	2.345	2.380	2.376
G_b	1.03	1.03	1.03	1.03
G_{se}	2.644	2.644	2.760	2.725
G_{sb}	2.618	2.618	2.734	2.699
CF	0.026	0.026	0.026	0.026
Bulk Density	142.4	146.3	148.5	148.3
Density at N_{ini}	-	134.2	134.0	133.1
% passing No. 200	5.64	5.64	12.28	5.96

Table B20. VDOT Volumetric Specifications for SM-12.5D Mixtures, Section A

Property	Specification Min.	Max.	Field-Field		Field-Lab		Lab-Lab		Design-Lab	
VTM (%)	2.5	5.5	5.8	Fail	3.2	Pass	5.2	Pass	4.8	Pass
VMA (%)	12	-	18.0	Pass	15.7	Pass	18.1	Pass	16.8	Pass
VFA (%)	62	80	67.8	Pass	79.8	Pass	71.4	Pass	71.4	Pass
% Density at N_{ini}	-	89	-	-	88.8	Pass	85.6	Pass	85.5	Pass
F/A ratio	0.6	1.3	1.0	Pass	1.0	Pass	2.2	Fail	1.1	Pass

Table B21. Volumetric Properties for SMA-12.5 Mixtures, Section L

Property	Field-Field	Field-Lab	Lab-Lab	Design-Lab
% Asphalt	6.80	6.80	6.44	6.33
G_{mm}	2.402	2.402	2.402	2.415
G_{mb}	2.226	2.359	2.359	2.359
G_b	1.03	1.03	1.03	1.03
G_{se}	2.661	2.661	2.644	2.657
G_{sb}	2.631	2.631	2.614	2.627
CF	0.03	0.03	0.03	0.03
Bulk Density	138.9	147.2	147.2	147.2
Density at N_{ini}	-	134.5	134.1	132.0
% passing No. 200	11.25	11.25	11.71	11.67

Table B22. VDOT Volumetric Specifications for SMA-12.5 Mixtures, Section L

Property	Specification Min.	Specification Max.	Field-Field		Field-Lab		Lab-Lab		Design-Lab	
VTM (%)	2.5	5.5	7.3	Fail	1.8	Fail	1.8	Fail	2.3	Fail
VMA (%)	12		21.1	Pass	16.4	Pass	15.6	Pass	15.9	Pass
VFA (%)	62	80	65.3	Pass	89.0	Fail	88.5	Fail	85.3	Fail
% Density at N_{ini}	-	89	-	-	89.7	Fail	89.5	Fail	87.6	Pass
F/A ratio	0.6	1.3	1.8	Fail	1.8	Fail	1.9	Fail	2.0	Fail